Naval Research Laboratory
Washington, DC 20375-5350

NRL/MR/7130-xxxxxxxxxxx

Effects of Target Corrosion/Bio-fouling on EMI & Structural Acoustic Signatures in Underwater Environments – Acoustic Component
Final Report to SERDP
MR-2500

J. A. Bucaro[1]

[1]*On-Site Contractor with Excet, Inc.*
Springfield, VA 2215

A. Sarkissian[2]

[2]*On-Site Contractor with Sotera KeyW*
Columbia, MD 21046

B.H. Houston and M. Saniga

Naval Research Laboratory
Washington, DC 20375

June 1, 2017

TABLE OF CONTENTS

LIST OF FIGURES 3
KEYWORDS 5
ACKNOWLEDGEMENTS 5
ABSTRACT 7
OBJECTIVE 9
BACKGROUND 9
MATERIALS AND METHODS 10
Bio-Fouling of Uxo Targets 11
Corrosion of UXO Targets 13
RESULTS AND DISCUSSION 13
Acoustic Measurements 13
Low Frequency Studies 14
High Frequency Studies 26
CONCLUSIONS AND IMPLICATIONS FOR FUTURE RESEARCH/IMPLEMENTATION 34
LITERATURE CITED 35

LIST OF FIGURES

Figure 1. Target strength (TS) vs frequency (semi-log) and aspect angle - acoustic color - for an epoxy-filled 5inch rocket. Measured (left); Rigid body response (right).

Figure 2. Photos of the 155mm Howitzer shell and 5 inch rocket.

Figure 3. (Left) 155mm Howitzer shell, (center) 5-inch rocket, and (right) test setup on dock at Englewood, FL site.

Figure 4. 155mm shell: (left) clean shell; (center) after 16 weeks in bio fouling site; (right) blow up of upper right.

Figure 5. 5 inch shell: (left) clean shell; (center) after 16 weeks in bio fouling site; (right) blow up of upper right.

Figure 6. Shells after accelerated anodical polarization in a bath of 0.05M NaCl for a week simulating ~3 months of seawater exposure. (left) 5 inch shell; (right) 155mm shell.

Figure 7. NRL 1M gallon structural acoustic pool facility.

Figure 8. Compact range configuration: (upper left) high frequency piston source; (lower left) low frequency near field array source.

Figure 9. Measured acoustic color spectra for the clean and bio-fouled shells: (upper) five inch shell; (lower) 155mm shell.

Figure 10. TS vs frequency for 5 inch shell: (Blue) clean; (Red) bio-fouled; (Green) theory for 1.4" radius rigid disc.

Figure 11. TS vs frequency for 155mm shell: (Blue) clean; (Red) bio-fouled; (Green) theory for 2" radius rigid disc.

Figure 12. TS vs frequency for 5inch shell: (Blue) clean; (Red) bio-fouled; (Green) theory for 2.5" radius rigid disc.

Figure 13. TS vs frequency for 155mm shell: (Blue) clean; (Red) bio-fouled; (Green) theory for 2.62" radius rigid disc.

Figure 14. TS vs frequency for 5inch shell: (Blue) clean; (Red) bio-fouled; (Green) theory for finite rigid cylinder.

Figure 15. TS vs frequency for155mm shell: (Blue) clean; (Red) bio-fouled; (Green) theory for finite rigid cylinder.

Figure 16. TS vs frequency for 5inch shell: (Blue) clean; (Red) bio-fouled; (Green) theory for1.4" radius rigid disc.

Figure 17. TS vs frequency for155mm shell: (Blue) clean; (Red) bio-fouled; (Green) theory for 2" radius rigid disc.

Figure 18. Low frequency correlation co-efficient between TS of target 1 at θ_i and target 2 at θ_j.

Figure 19. The performance (scaled combinatorial output) of the RVM classification algorithm trained generatively on even ½ degree angles using maximum pressure magnitude, mean pressure magnitude, pressure derivative maximum, and mean pressure

derivative maximum for 5 inch and 155mm shells and tested on odd ½ degree angles for the 5 inch and 155mm shells and every degree for the bio-fouled targets and 6 non-UXO targets.

Figure 20. The performance (scaled combinatorial output) of the RVM classification algorithm trained generatively on even ½ degree angles using acoustic color for 5 inch and 155mm shells and tested on odd ½ degree angles for the 5 inch and 155mm shells and every degree for the bio-fouled targets and 6 non-UXO targets.

Figure 21. Measured acoustic color spectra for the clean and corroded shells: (upper) five inch shell; (lower) 155mm shell.

Figure 22. TS vs frequency for 5inch shell: (Blue) clean; (Red) corroded; (Green) theory for 1.4" radius rigid disc.

Figure 23. TS vs frequency for 5inch shell: (Blue) clean; (Red) corroded; (Green) theory for 2.5" radius rigid disc.

Figure 24. TS vs frequency for 5inch shell: (Blue) clean; (Red) corroded; (Green) theory finite rigid cylinder.

Figure 25. TS vs frequency for 5inch shell: (Blue) clean; (Red) corroded; (Green) theory for 2.5" radius rigid disc.

Figure 26. TS vs frequency for 155mm shell: (Blue) clean; (Red) corroded; (Green) theory for 2" radius rigid disc.

Figure 27. TS vs frequency for 155mm shell: (Blue) clean; (Red) corroded; (Green) theory for 2.62" radius rigid disc.

Figure 28. TS vs frequency for 155mm shell: (Blue) clean; (Red) corroded; (Green) theory for rigid finite cylinder.

Figure 29. TS vs frequency for 155mm shell: (Blue) clean; (Red) corroded; (Green) theory for 2" radius rigid disc.

Figure 30. Measured acoustic color spectra for the clean and bio-fouled shells: (upper) five inch shell; (lower) 155mm shell.

Figure 31. TS vs frequency for 5"shell: (Blue) clean; (Red) bio-fouled; (Green) theory for 1.4" radius rigid disc.

Figure 32. TS vs frequency for 5" shell: (Blue) clean; (Red) bio-fouled; (Green) theory for 2.5" radius rigid disc.

Figure 33. TS vs frequency for 5"shell: (Blue) clean; (Red) bio-fouled; (Green) theory for finite rigid cylinder.

Figure 34. TS vs frequency for 155mm shell: (Blue) clean; (Red) bio-fouled; (Green) theory for 2" radius rigid disc.

Figure 35. TS vs frequency for 155mm shell: (Blue) clean; (Red) bio-fouled; (Green) theory for 2.62" radius rigid disc.

Figure 36. TS vs frequency for 155mm shell: (Blue) clean; (Red) bio-fouled; (Green) theory for finite rigid cylinder.

Figure 37. High frequency correlation co-efficient between TS of target 1 at θ_i and target 2 at θ_j.

Figure 38. Measured acoustic color spectra for the clean and corroded shells: (upper) five inch shell; (lower) 155mm shell.

Figure 39. TS vs frequency for 5" shell: (Blue) clean; (Red) corroded; (Green) theory for 1.4" radius rigid disc.

Figure 40. TS vs frequency for 5" shell: (Blue) clean; (Red) corroded; (Green) theory for 2.5" radius rigid disc.

Figure 41. TS vs frequency for 5" shell: (Blue) clean; (Red) corroded; (Green) theory for rigid finite cylinder.

Figure 42. TS vs frequency for155mm shell: (Blue) clean; (Red) corroded; (Green) theory for 2" radius rigid disc.

Figure 43. TS vs frequency for 155mm shell: (Blue) clean; (Red) corroded; (Green) theory for 2.62" radius rigid disc.

Figure 44. TS vs frequency for 155mm shell: (Blue) clean; (Red) corroded; (Green) theory for finite rigid cylinder.

ACRONYMS

LDV	Laser Doppler Vibrometry
LSA	Laboratory for Structural Acoustics
NAH	Nearfield Acoustic Holography
NRL	Naval Research Laboratory
RVM	Relevance Vector Machine
SA	Structural Acoustic
S/N	Signal to Noise
3D	Three Dimensional
TS	Target Strength
UXO	Unexploded Ordnance

KEYWORDS

Underwater Buried UXO, structural acoustic target identification, sonar UXO detection, bio-fouled UXO, corroded UXO

ACKNOWLEDGEMENTS

This work was performed under direct support from the SERDP Program Office. We would like to acknowledge the very positive and encouraging program management role played by Dr. Herb Nelson, former SERDP Program Manager for Munitions Response now director of SERDP &

ESTCP. We would also like to acknowledge the significant role played by Dr. Daniel Steinhurst, Nova Research @ NRL, Dr. Matthew Strom, NRL, Dr. Thomas Bell, Leidos @ NRL, and Dr. Bruce Barrow, Leidos @ NRL who conduced the EMI component of this program and who carried out the bio-fouling and corroding of the two UXO targets.

ABSTRACT

Objective: Many active and former military installations have ordnance ranges/training areas with adjacent water environments containing unexploded ordnance (UXO) due to wartime activities, dumping, and accidents. SERDP goals require the development of technologies able to detect and classify UXO, and a number of SERDP projects have been developing structural acoustic (SA) feature-based underwater sonars that can detect and localize buried (and proud) targets separating the detections into UXO vs non-UXO. These and related efforts have generated a growing library of what are called "acoustic color" data bases (acoustic scattering versus frequency and aspect) for a variety of UXO targets. It is from these acoustic color maps that classification features are derived. For the most part, these data bases do not include targets that are corroded or bio-fouled so that there is little understanding regarding how structural acoustic features might be altered by these effects. Further, the SA sonar methodology includes 3D acoustic imagery where large synthetic apertures created by the sonar's motion allow modest spatial resolution even at the low SA frequencies so that the impact on imagery of bio-fouling and corrosion is also of interest. Our objective here is to generate a carefully controlled data base determining the effects of corrosion and bio-fouling on a UXO target's echo characteristics i.e. on "acoustic color" from which both the classification features and images are generated.

Technical Approach: The detailed frequency/angle structure in the measured acoustic color map provides effective "fingerprinting" features for the classification algorithm. Here we measure these color maps for two UXO – a 5" rocket and a 155mm shell both filled with an epoxy resin – and then repeat the measurements after the targets have experienced bio-fouling and then corrosion. Further, we attempt to determine how the various structural acoustic mechanisms which lead to these features are affected by the bio-fouling or corrosion. For example, the color map for a rigid rocket is a good approximation for the specular scattered component. The specular component is of interest since it is used to form an acoustic image providing direct classification information such as size and shape. We will attempt to determine how the various mechanisms including circumferential and axial elastic or creeping waves travelling in the shell casing are affected. Finally, we assess the effect of the bio-fouling and corrosion on the performance of our typical RVM classification algorithm. The acoustic scattering measurements are carried out in NRL's state-of-the-art Laboratory for Structural Acoustics Facility. The measurements are made over the broad frequency band from 2 kHz to 160 kHz and over a full 360 degrees in steps of one half or one degree. The band is covered by using two facility configurations, one the high frequency arrangement which utilizes a relatively small source and receiver and the other the low frequency system which deploys a large near-field source array to project a plane wave on the nearby target. After baseline scattering measurements are carried out on the "clean" targets, the UXO are exposed for 16 weeks underwater at an at-sea fouling location in Englewood, FL which contains an aggressive fouling community with a high percentage of hard fouling species so that significant bio-fouling occurred during this relatively short time. After completing acoustic measurements on the bio-fouled UXO, the shells are cleaned and readied for accelerated corrosion in order to produce magnetite/Hermatite corrosion layers. To accomplish this, the munitions are anodically polarized in a bath of 0.05M NaCl for a week long period such that the corrosion rate is accelerated, simulating ~3 months of seawater exposure. After the corrosion process is completed, the acoustic measurements are repeated once more.

Results: The baseline measurements were analyzed in terms of basic echo mechanisms which included specular scattering from shell ends and cylindrical surfaces, circumferential Rayleigh wave and compressional wave ring resonances, axial compressional and creeping wave interference with specular scattering, elastic wave generation in filler due to phase matching, etc. Low frequency (structural acoustic domain) acoustic scattering measurements made on the two bio-fouled shells together with subsequent analysis demonstrated the following. Overall the bio-fouling has affected the scattering levels a small amount but not the overall acoustic color frequency-angle spectra. The level changes, amounting to on average less than 2dB for the 5 inch shell and about 5dB for the 155mm shell, would result in a corresponding drop in signal-to-noise and in turn the related detection ranges. However, the robustness of the acoustic color spectra bodes well for the performance of our RVM classification algorithms. In this regard, both the acoustic color features and certain pressure magnitude features maintain good UXO classification performance against the set of six non-UXO targets. In particular, pressure magnitude features were shown to separate 4 of 6 false targets from bio-fouled UXO whereas acoustic color features separated all 6 of 6 false targets from bio-fouled UXO. Further, we found that bio-fouling tends to attenuate some axial creeping (~ 1.2 - 1.7 kHz) and circumferential elastic waves (~ 6 kHz – 12 kHz) reducing fine structure. This is especially true for 155mm shell. Reduced levels of fine structure are expected to lead to sharper low frequency images since these mechanisms lead to echo time elongation which corrupts the time-delay beamforming processing used in imaging. Regarding the small amount of corrosion achieved in our laboratory which attempts to accelerate the corrosion process, except for the apparently anomalous change for the echo from the front and back of both shells at the lowest frequencies and the significant effect on the circumferential Rayleigh wave for the five inch shell, there is as expected no change of any consequence caused by this thin corrosion layer at the low structural acoustic frequencies. We conclude without specifically demonstrating it that there would be little impact on acoustic detection ranges, classification performance, or maximum burial depth caused by this thin corrosion layer. Regarding the measurements made over the high frequency (conventional imaging regime), the specular echo is affected only in a minor way by bio-fouling, and much of the fine structure due to creeping or elastic axial/circumferential waves is washed out (less true for 155mm shell). Finally, the thin corrosion layer has no noticeable effect on acoustic response over almost the entire band.

Benefits: A number of SERDP Projects have been exploring structural acoustics (SA) based sonar for detection/classification of underwater UXO which offer significant advantages over the more conventional acoustic imaging approaches including a diverse set of spatial and spectral structural acoustic “fingerprints” leading to high probability of detection, low false alarm rates and low frequency sediment penetration permitting buried target prosecution. Further, the SA approach allows the formation through SAS processing of complementary three dimensional images of the sediment volume and of any targets buried therein having sufficient resolution to allow determination of the approximate target size, burial depth, and burial angle. The combination of this information provides the necessary information regarding the presence, location, and identification of underwater UXO for effective inspection at sites requiring remedial action. Until now, there has been little or no information collected regarding the effect of seawater bio-fouling or corrosion on the acoustic color maps used to generate the SA features and images. This project has established that significant bio-fouling and/or thin corrosion layers have little impact on acoustic color or on the related classification approaches.

OBJECTIVE

Many active and former military installations have ordnance ranges/training areas with adjacent water environments containing unexploded ordnance (UXO) due to wartime activities, dumping, and accidents. SERDP goals require the development of technologies able to detect and classify UXO, and a number of SERDP projects[1-8] have been developing structural acoustic (SA)[9] feature-based underwater sonars that can detect and localize buried (and proud) targets separating the detections into UXO vs non-UXO. These and related efforts have generated a growing library of what are called "acoustic color" data bases (acoustic scattering versus frequency and aspect) for a variety of UXO targets. It is from these acoustic color maps that classification features are derived. For the most part, these data bases do not include targets that are corroded or bio-fouled so that there is little understanding regarding how structural acoustic features might be altered by these effects. Further, the SA sonar methodology includes 3D acoustic imagery[10,11] where large synthetic apertures created by the sonar's motion allow modest spatial resolution even at the low SA frequencies so that the impact on imagery of bio-fouling and corrosion is also of interest. Our objective here is to generate a carefully controlled data base determining the effects of corrosion and bio-fouling on a UXO target's echo characteristics i.e. on "acoustic color" from which both the classification features and images are generated.

BACKGROUND

Many active and former military installations have ordnance ranges/training areas with adjacent water environments in which unexploded ordnance (UXO) now exists due to wartime activities, dumping, and accidents. SERDP goals require the development of innovative technologies able to separate UXO from false targets and to discriminate amongst UXO targets themselves. The sonar configuration of interest in this program is the shorter range, down-looking system which uses mono-static and bi-static echo responses over relatively limited angular apertures[5]. Because the downward-directed acoustic energy intercepts the water-sediment interface at angles well above the critical angle, sound penetration into the sediment is not an issue for most bottom types. A number of SERDP Projects[1-8] have been exploring structural acoustics (SA)[9] based sonar for detection/classification of underwater UXO which offer significant advantages over the more conventional acoustic imaging approaches including a diverse set of spatial and spectral structural acoustic "fingerprints" leading to high probability of detection, low false alarm rates and low frequency sediment penetration permitting buried target prosecution. Further, the SA approach allows the formation through SAS processing of complementary three dimensional images of the sediment volume and of any targets buried therein having sufficient resolution to allow determination of the approximate target size, burial depth, and burial angle.[10-14] The combination of this information provides the necessary information regarding the presence, location, and identification of underwater UXO for effective inspection at sites requiring remedial action. Until now, there has been little or no information collected regarding the effect of seawater bio-fouling or corrosion on the acoustic color maps used to generate the SA features and images. This project will collect data which for the first time will has established what major impact significant bio-fouling and/or thin corrosion layers have might have on acoustic color or on the related classification approaches.

MATERIALS AND METHODS

A number of SERDP Projects (MR-1513[1-5], MR-1665[6], MR-2103[7-10], MR-2230[11], etc.) have been exploring structural acoustics (SA) based sonar methodology[12] for detection and classification of underwater unexploded ordnance (UXO). The structural acoustic approach to target detection and identification offers significant advantages over these more conventional acoustic approaches which rely only on the formation of high resolution images. These advantages include a diverse set of spatial and spectral structural acoustic "fingerprints" leading to high probability of detection, low false alarm rates and low frequency sediment penetration permitting buried target prosecution. These and related efforts have generated a growing library of what are called "acoustic color" data bases[13] (acoustic scattering versus frequency and aspect) for a variety of UXO targets. It is from these acoustic color maps that classification features[11,14,15] are derived. For the most part, these data bases do not include targets that are corroded or bio-fouled so that there is little understanding regarding how structural acoustic features might be altered by these effects. Further, the SA sonar methodology often includes the formation of 3D acoustic imagery where large synthetic apertures created by the sonar vehicle's motion allow modest spatial resolution even at the low SA frequencies[16,17] so that the impact on imagery of bio-fouling and corrosion is also of interest.

Our objective here is to generate a carefully controlled data base determining the effects of corrosion and bio-fouling on a UXO target's echo characteristics i.e. on "acoustic color" from which both the classification features and images are generated. We show on the left in Fig. 1 the acoustic color map measured for a five inch rocket filled with an epoxy resin.[13] On the right is shown the acoustic color map that would result were the target perfectly rigid, i.e. the case in which no acoustic energy penetrates the target. The detailed frequency/angle structure in the measured map on the left provides effective "fingerprinting" features for the classification algorithm. In the following study, we measure these color maps for two UXO – a five inch rocket and a 155mm shell both filled with an epoxy resin – and then repeat the measurements after the targets have experienced bio-fouling and then corrosion. Further, we attempt to determine how the various structural acoustic mechanisms which lead to these features are affected by the bio-fouling or corrosion. As an example, the color map on the right in Fig. 1 for a *rigid* rocket is a good approximation for the specular scattered component in the acoustic echo. The specular component is of interest since it is used to form an acoustic image which provides direct classification information such as size and shape. We will attempt to determine how the various other mechanisms including circumferential and axial elastic or creeping waves travelling in the shell casing are affected. Finally, we assess the effect of the

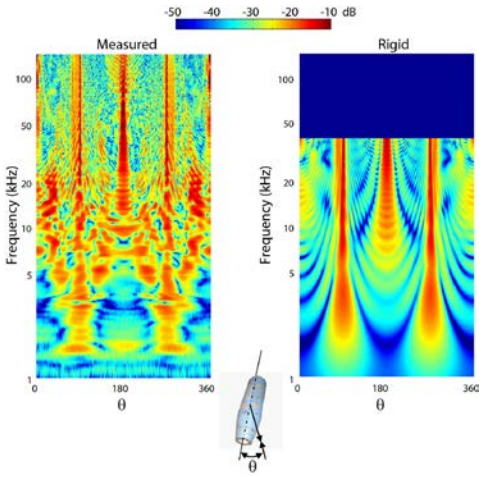

Figure 1. Target strength (TS) vs frequency (semi-log) and aspect angle - acoustic color - for a epoxy-filled 5inch rocket. Measured (left); Rigid body response (right).

bio-fouling and corrosion on the performance of our typical RVM[7,14,15,20] classification algorithm.

The acoustic scattering measurements were carried out in NRL's Laboratory for Structural Acoustics Facility, a state-of-the-art, 1M gallon, controlled and highly instrumented in-ground pool. The measurements were made over the broad frequency band shown in Fig. 1, i.e. 2 kHz to 160 kHz and over a full 360 degrees in steps of one half or one degree. The band is covered by using two facility configurations[13,21], one the high frequency arrangement which utilizes a relatively small source and receiver and the other the low frequency system which deploys a large near-field source array to project a plane wave on the nearby target.

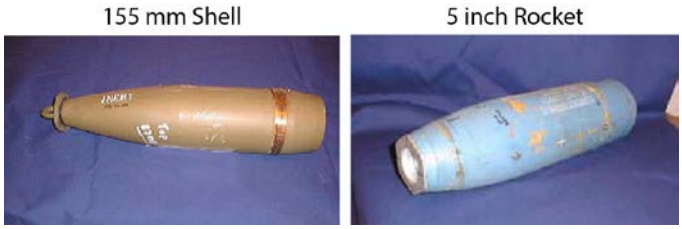

Figure 2. Photos of the 155mm Howitzer shell and 5 inch rocket.

Bio-Fouling of Uxo Targets

After baseline scattering measurements were carried out in the NRL Building 5 Structural Acoustic Pool Facility on the "clean" targets (Fig. 2), the UXO were exposed for 16 weeks underwater at an at-sea fouling location in Englewood, FL to support hard fouling testing[22]. The Englewood site contains an aggressive fouling community with a high percentage of hard fouling species so that significant bio-fouling occurred during this relatively short time. The simple deployment arrangement is shown in Fig. 3.


Figure 3. – (left) 155mm Howitzer shell, (center) 5-inch rocket, and (right) test setup on dock at Englewood, FL site.

The resulting bio-fouling achieved in the sixteen week submersion is shown in Fig. 4 together with the clean target for the 155mm shell. As can be seen, a significant amount of biological material has "grown" onto the shell. Similarly, the bio-fouled five inch rocket together with the clean target is shown in Fig 5. This bio-fouling is typically observed in barnacle (cyprid) and tubeworm (spirorbid) settlement and growth[22].

Figure 4. 155mm shell: (left) clean shell; (center) after 16 weeks in biolfouling site; (right) blow up of upper right.

Figure 5. 5 inch shell: (left) clean shell; (center) after 16 weeks in biolfouling site; (right) blow up of upper right.

Corrosion of UXO Targets

After completing acoustic measurements on the bio-fouled UXO, the shells were cleaned and readied for accelerated corrosion in order to produce magnetite/Hermatite corrosion layers. To accomplish this, the munitions were anodically polarized in a bath of 0.05M NaCl for a week long period such that the corrosion rate was accelerated, simulating ~3 months of seawater exposure[22]. An anodic polarization causes the entire surface of the munition to behave like an anode, the half of the redox reaction that causes material loss. A combination of Hematite (α-$F_{e2}O_3$) and magnetite ($F_{e3}O_4$) make up the corrosion product on the surface which is electrically conducting and magnetic. Magnetic properties of iron oxide minerals change according to their grain size with the critical single domain size for magnetite being 0.05–0.084 μm and for hematite 15 μm.

Figure 6. Shells after accelerated anodical polarization in a bath of 0.05M NaCl for a week simulating ~3 months of seawater exposure. (Left) 5 inch shell; (Right) 155mm shell.

The level of corrosion we obtained is shown in the photographs of Fig. 6. This level of corrosion although accelerated was in effect more relevant to induction than to acoustics. Although the corrosion layer is very thin, it can produce a significant effect on the eddy current response and thus the induction signals. However, the thin corrosion layer would be expected to affect acoustic scattering only in a minor way and then predominately at very high frequencies well beyond the structural acoustic band. In this regard, future acoustic work regarding corrosion should consider mechanically removing chunks of metal uniformly over the UXO surface as a means of achieving more significant corrosion of the type expected over very long submersion times.

RESULTS AND DISCUSSION

Acoustic Measurements

The acoustic scattering measurements were carried out at the Laboratory for Structural Acoustics (LSA) at NRL (see Figure 7) which is a state-of-the-art underwater acoustic research laboratory unique in the world[13,21]. The LSA infrastructure includes a large cylindrical one million gallon (55-ft diameter x 50-ft deep) de-ionized water tank located in Building 5 at NRL. This tank is vibration isolated, temperature controlled, and heavily instrumented with in-water precision robots for nearfield acoustic holography (NAH), laser

Figure 7. NRL 1M gallon structural acoustic pool facility.

Doppler vibrometry (LDV), and compact range measurements.

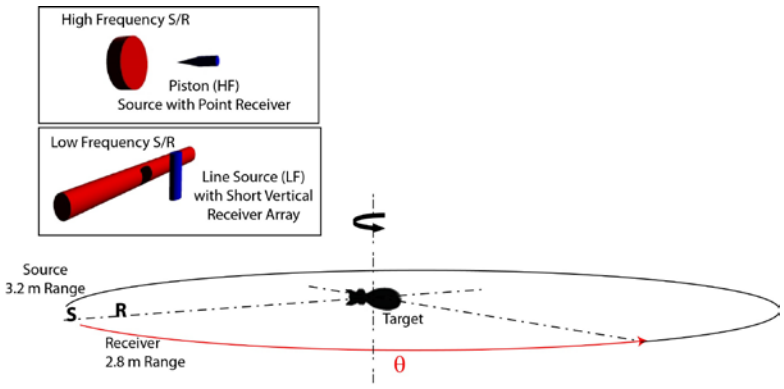

Figure 8. Compact range configuration: (upper left) high frequency piston source; (lower left) low frequency near field array source.

The measurements reported here were conducted with the facility in its compact scattering range mode[13,21] as shown in Fig. 8. Each UXO target was suspended at mid-depth in the tank together with the source and receiver. Two sources were used for these experiments. The first source is a 3 meter long nearfield line array mounted horizontally. The line array generates a broadband pulse approximately 1 ms in duration and covers the band from 1 – 25 kHz. The spatial uniformity of the line array output is such that it emulates a farfield plane wave ensonification. The receiver used in these experiments was a vertical line array that is also suspended at the mid-depth of the tank. A second piston-like source is used to collect data in the band from 8 kHz – 160 kHz. The measurement system is designed for collection of both monostatic and bistatic scattering data. However, for the measurements reported here, only the monostatic configuration was used, i.e. the source and receiver fall along the same bisector to the target center. The scattered echo response was measured 2.7 meters from the target in 1 degree increments over 360 degrees. The data was processed to recover full complex scattering cross-sections expressible as target strength referenced to 1 meter. In this method, the time domain scattered data from the target at a given aspect angle is cleaned to remove unwanted reflections not associated with a target return, is Fourier transformed, and then normalized by a reference measurement.

Low Frequency Studies

The low frequency measurements for the shells both before and after bio-fouling are shown in Fig. 9. These are target strength (TS) displays versus frequency and angle[13]. As such, they are proportional to acoustic color. As can be seen, overall the bio-fouling has affected the scattering levels a small amount but not the overall acoustic color frequency-angle spectra. The level changes, amounting to on average less than 2dB for the 5 inch shell and about 5dB for the 155mm shell, would result in a corresponding drop in signal-to-noise and in turn the related detection ranges. However, the robustness of the acoustic color spectra bodes well for the performance of our RVM classification algorithms.

Shown in Fig. 10 through Fig. 15 are TS plots versus frequency for the three commonly discussed and analyzed target aspects, 0° (front), 90° (side or beam), and 180° (back). In discussing the TS at these three aspects, we refer to several theoretical expressions relevant to

important mechanisms involved in the scattering process. The first describes the specular scattering from a flat, rigid disc of area A versus wavelength λ and angle θ[23]:

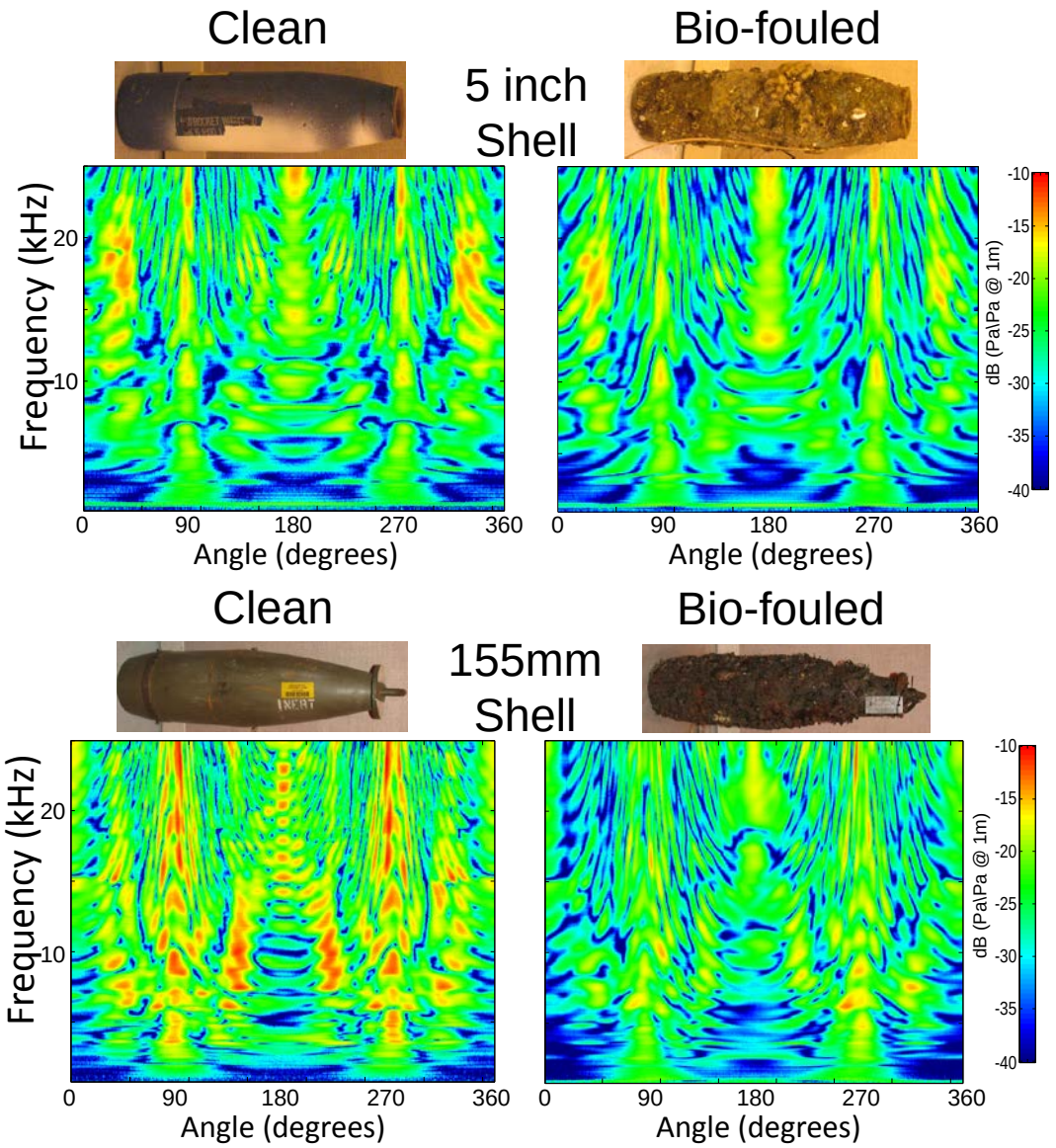

Figure 9. Measured acoustic color spectra for the clean and bio-fouled shells: (upper 5 inch shell; lower 155mm shell.

$$TS = 20\log\left\{A\cos\frac{\theta}{\lambda}\right\} \tag{1}$$

The second relates to the scattering from a finite, acoustically rigid cylinder of radius a and length L versus acoustic wavenumber k[23]

$$TS = 20\log\left\{\frac{L}{2}\left[\frac{ka}{\pi}\right]^{1/2}\right\}. \tag{2}$$

The third refers to the well-known ring-resonance[24] drop-outs with frequency at beam aspects caused by the destructive interference between the 180 degree phase-shifted specular echo and radiation from elastic waves having circumnavigated the shell at wave speed $C_{elastic}$

$$f_{\text{ring res}} = n\,\frac{C_{elastic}}{(2\pi a)} \tag{3}$$

The final simple expression relates to the frequency beats Δf caused by the interference between a specular echo and one delayed by a time interval L/C or d/C where L is cylinder length (when the second echo is created by a wave traveling down the length of the cylinder and reflected back by the end discontinuity) and d is the separation between two specular surfaces and C is the sound speed

$$\Delta f = \frac{C}{2L},\ \frac{C}{2d} \tag{4}$$

Returning to Fig. 10 for the 0° aspect case, we see that the overall level and frequency dependence is described well by Eq. (1) for scattering from a disc of the size of the 5inch rocket front end. Further, the 1.7 kHz fine structure is also adequately predicted by Eq.(4) which in this case would describe the creeping wave[24] travelling at the sound speed down the length of the target, reflecting from the end discontinuity, and interfering with the specular reflection after travelling back to the front. Of greater importance is the observation that the significant amount of bio-fouling has not had much effect on the either the overall scattering or on the individual mechanisms described above.

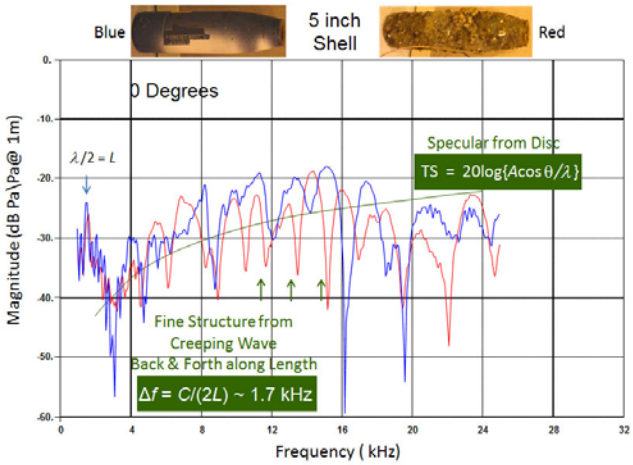

Figure 10. TS vs frequency for 5 inch shell: (blue) clean; (Red) biofouled; (green) theory for 1.4" radius rigid disc.

These observations and conclusions are also applicable to the 0° case for the 155mm shell shown in Fig. 11 with one difference being that the overall scattering level for the bio-fouled shell has now dropped by on average about 3-5 dB. We note, however, that the fine structure we attribute to interference with the axially-travelling creeping wave has not been changed significantly even though the wave has travelled twice the cylinder length.

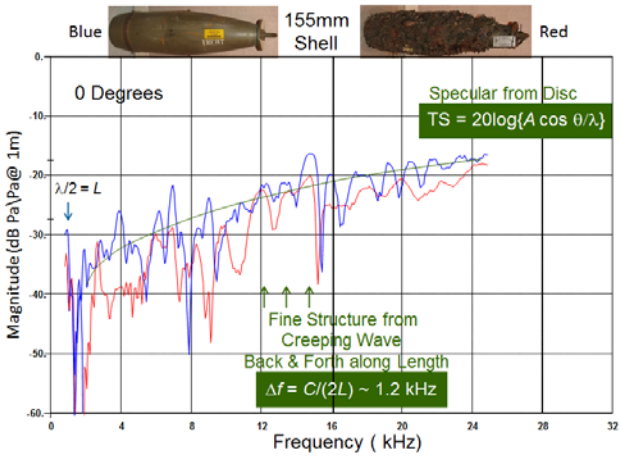

Figure 11. TS vs frequency for 155mm shell: (Blue) clean; (Red) bio-fouled; (Green) theory for 2" radius rigid disc.

Next, consider the response from the back of the targets, i.e. 180°. These are

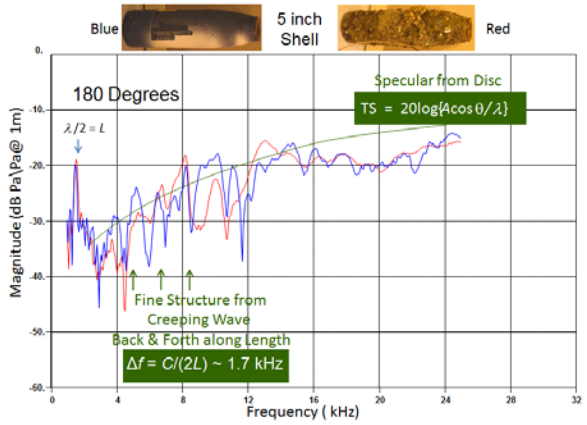

Figure 12. TS vs frequency for 5inch shell: (Blue) clean; (Red) bio-fouled; (Green) theory for 2.5" radius rigid disc.

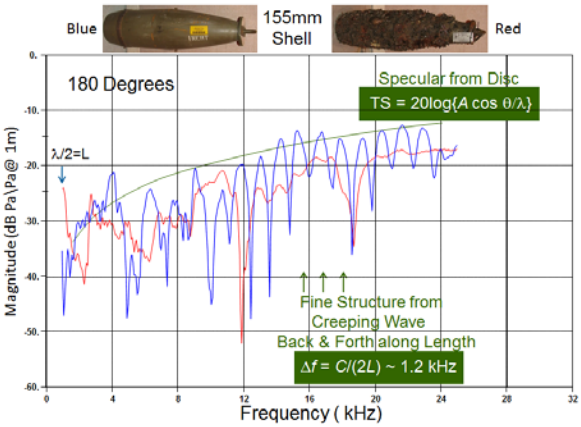

Figure 13. TS vs frequency for 155mm shell: (Blue) clean; (Red) bio-fouled; (Green) theory for 2.62" radius rigid disc.

shown in Fig. 12 and Fig 13. The situation at the rear aspect is similar to

that found for the front end. Again we see that the overall level and frequency dependence is described well by Eq.(1) for scattering from a rigid disc the size of the 5 inch rocket and 155mm ends. Further, the 1.7 kHz and 1.2 kHz fine structure is also adequately predicted by Eq.(4) which in this case would describe the creeping wave travelling at the sound speed down the length of the target, reflecting from the end discontinuity, and interfering with the specular reflection after travelling back to the front. In this case, the fine-structure appears greater for the clean 155mm shell than for the 5 inch rocket, whereas the reverse was true for 0°. More important is the observation that the significant amount of bio-fouling has not had much effect on the overall scattering level or frequency shape. However, in this case, it appears to have

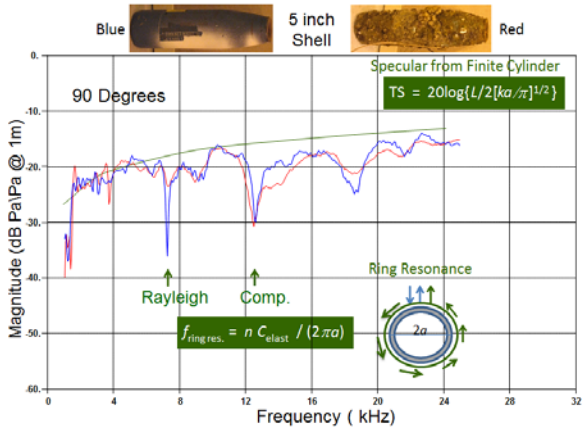

Figure 14. TS vs frequency for 5inch shell: (Blue) clean; (Red) bio-fouled; (Green) theory for finite rigid cylinder.

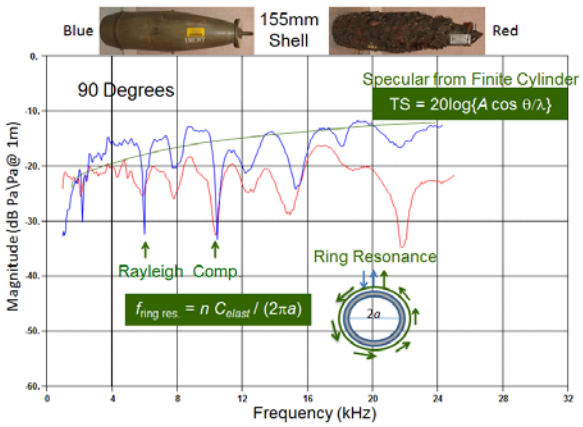

Figure 15. TS vs frequency for155mm shell: (Blue) clean; (Red) bio-fouled; (Green) theory for finite rigid cylinder.

noticeably reduced the creeping wave contribution, certainly in the case of the 155mm shell.

Next we consider the beam responses at 90° as shown in Fig. 14 and Fig. 15. For both targets, the shape and level of the beam response is as predicted by Eq. (2) with a small level disagreement at the higher frequencies of the 5 inch case. Further, two of the observed ring

resonances for both targets are as predicted by Eq. (3) where the first relates to the Rayleigh wave[25] speed and the second to the plate compressional[26] speed. Regarding the effect of the bio-fouling on both targets, we can see that there is almost no change for the depth of the compressional ring resonance but a significant change for the Rayleigh wave resonance. Apparently the bio-fouling has a large effect on the Rayleigh wave which has a significant radial displacement. On the other hand, the compressional wave having a relatively small radial displacement has not been affected significantly. For the 155mm shell, the bio-fouling has led to an overall 5 dB drop in the levels as well as the afore-mentioned filling-in of the first Rayleigh wave ring resonance dip.

Next, we consider what we consider to be a special case, i.e. 45°. We consider this quartering aspect case special because we believe that at this angle phase matching can take place between the incident wave in water and a compressional wave travelling in the epoxy filler[5]. For an epoxy sound speed of 2100m/s, the phase matching angle $\theta = \cos^{-1}(1500ms^{-1}/2100ms^{-1}) = 44°$. That

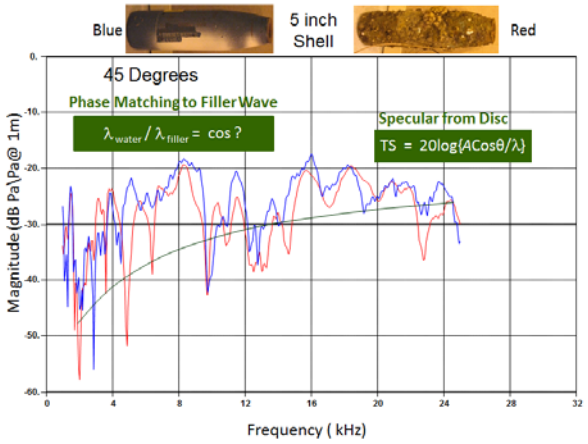

Figure 16. TS vs frequency for 5inch shell: (Blue) clean; (Red) bio-fouled; (Green) theory for 1.4" radius rigid disc.

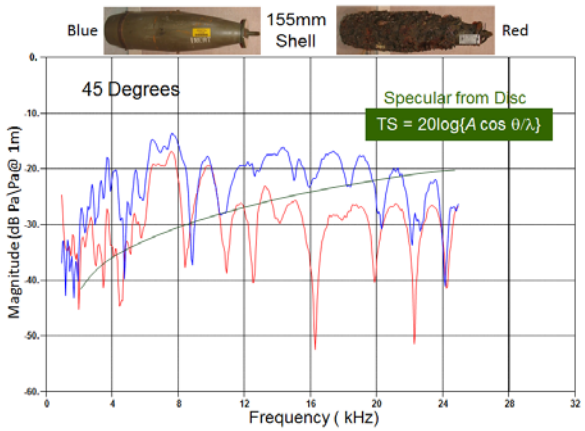

Figure 17. TS vs frequency for155mm shell: (Blue) clean; (Red) bio-fouled; (Green) theory for 2" radius rigid disc.

this mechanism leads to increases levels and frequency structure in the low frequency target strength has been noted in our previous publications[5].

We show in Fig. 16 and Fig. 17 the quartering responses for the 5 inch rocket and the 155mm shell, respectively. As can be seen, in both clean shell cases, the low frequency response is indeed higher than that predicted for scattering from a flat disc at 45°. Further, these interior elastic waves would reflect back from the ends producing fine structure with $\Delta f \sim 2.2$ kHz as is evident at the higher end of the frequency band. We have pointed out previously that this low frequency mechanism at quartering involving the shell interior material can aid in UXO classification. In that regard, it is encouraging that it does not appear to be impacted significantly by the bio-fouling introduced here for the 5 inch rocket and for the lower end of the band for the 155mm shell.

In summary, as supported by the results displayed in the acoustic color maps of Fig. 9, the bio-fouling has not produced changes of a magnitude or nature that would be expected to significantly impact the methods we expect to exploit for target classification, viz. 3-D imaging

and application of acoustic color-based RVM algorithms. Regarding the latter, we show later that there is little effect on RVM classification. Regarding imaging, the fact that there is some reduction in the influence on acoustic color of axial creeping waves and Rayleigh circumferential waves implies image resolution improvement since these mechanisms produce elongated echo time signals which corrupt images formed using time-delay beamforming. Further, the average decreases in the target strength are not sufficient to produce significant decreases in the target detection range including the depth at which buried targets could be prosecuted.

As further support for these conclusions, we show in Fig. 18 angle-angle correlation maps based on the low frequency TS data. These plots are generated by computing the correlation co-efficient between the target strengths for two targets at each angle integrated over the entire low frequency band. We take as the baseline correlated cases the same clean targets (1 and 2) which show a perfect correlation of 1 and as the baseline uncorrelated cases different targets either one of which is clean or bio-fouled (5 – 8). For the latter, we only show the correlation result for the two different clean targets (6). As can be seen, there remains a significant correlation diagonal for the two test cases, i.e. the clean versus bio-fouled 5 inch rocket (3) and the clean versus bio-fouled 155mm shell although the correlation co-efficient has dropped somewhat.

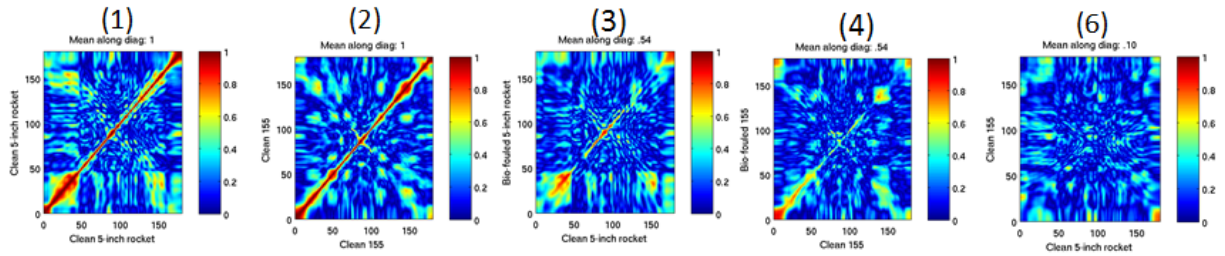

(1) Clean 5 inch shell vs clean 5 inch shell
(2) Clean 155mm shell vs clean 155mm shell

Baseline Cases: *Clear diagonals*

(3) Bio-fouled 5 inch shell vs clean 5 inch shell
(4) Bio-fouled 155mm shell vs clean 155mm shell

Test Cases: *Clear diagonals from 1 to ~ 0.54*

(5) Bio-fouled 155mmshell vs clean 5 inch shell
(6) Clean 155mm shell vs clean 5 inch shell
(7) Bio-fouled 155mm shell vs bio-fouled 5 inch shell
(8) Clean 155mm shell vs bio-fouled 5 inch shell

Baseline cases: No observable diagonals

Figure 18. Low frequency correlation co-efficient between TS of target 1 at θ_i and target 2 at θ_j.

Finally, we present a direct evaluation regarding the effect of the bio-fouling on the performance of our typical RVM classification algorithms. In the study, we include two data sets for the "clean" UXOs. The first labeled #1 refers to the measurements made on the UXOs prior to exposing them to bio-fouling. The second labeled #2 refers to measurements made years ago[13] on a different 5inch rocket and 155mm shell. In the following, we train an RVM algorithm

generatively[27] using the complete 360 degrees of acoustic scattering data for the two clean #1 UXOs measured every 1/2 degree over the band 2-24 kHz. In the first study case we use four features (maximum pressure magnitude, mean pressure magnitude, pressure derivative maximum, and mean pressure derivative maximum). The testing is carried out using the same features on clean #1 UXOs at every 1/2 degree, every odd 1/2 degree for bio-fouled #1 shells and every 1 degree for all others. For this test, the RVM scaled probability is determined over each of eighty 21 degree apertures stepped by ½ (or 1) degree at a time and then taking the product of the eighty P's raised to the 1/80 power. This is done over the full 360 degrees stepping the 80 degree sector 1 degree at a time and plotting a scaled version of $P(\theta_{sector})$ for each target as shown in Fig. 19.

In this result, we show testing results for the two sets of clean UXO targets: the 5 inch rocket and 155mm shell used in this study for which the target strength was measured before exposure to seawater and the same target types measured some years ago[13] in the same facility. The results for the two bio-fouled targets shown within the red contour fall just below the results for both sets of clean targets. For comparison, we show results for six non-UXO targets as listed. Four of these non-UXO targets fall well below those for the bio-fouled UXO. Two of the non-UXO – a metal sphere and a cinderblock – fall within the same levels as the bio-fouled targets.

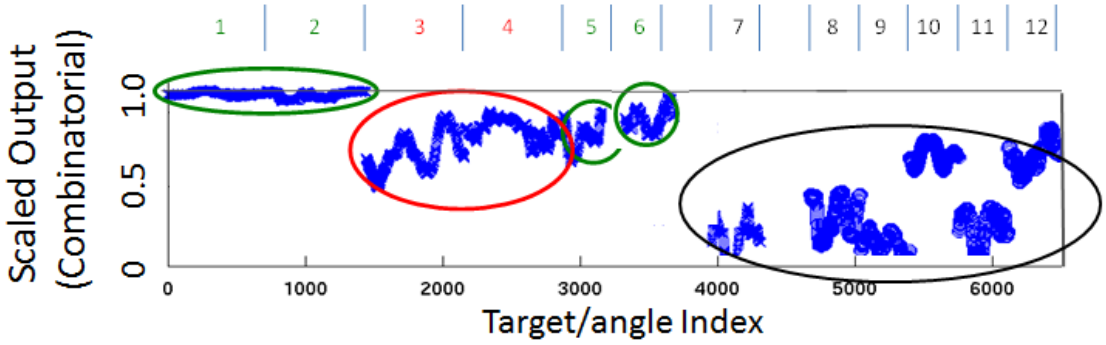

Targets for Baseline Testing

1) Clean 5 inch shell #1
2) Clean 155mm shell #1
5) Clean 5 inch shell #2
6) Clean 155mm shell #2

Bio-fouled Target Testing

3) Bio-fouled 5 inch shell
4) Bio-fouled 155mm shell

Non-UXO Testing

7) 25mm dummy cartridge
8) Rock #1
9) Drum
10) Metal sphere
11) Gas bottle
12) Cinderblock

Figure 19. The performance (scaled combinatorial output) of the RVM classification algorithm trained generatively on every ½ degree angles using maximum pressure magnitude, mean pressure magnitude, pressure derivative maximum, and mean pressure derivative maximum for 5 inch and 155mm shells and tested on every ½ degree angles for the 5 inch and 155mm shells and every degree for the bio-fouled targets and 6 non- UXO targets.

Next, we carry the above study using the acoustic color features rather than the four aforementioned pressure level – related features. The results are shown in the similar plot in Fig. 20 except that the testing on clean UXO is done every degree. In contrast to the results for the other features presented in Fig.19, here the RVM scaled output for the bio-fouled UXO falls

between the two sets of clean UXOs. However, the bio-fouled RVM output falls within the same bounds as that for the previous features in Fig. 19. Thus the fact that the result for the acoustic color feature is above that for the #2 clean UXO set suggests an issue with the #2 clean UXO set results rather than with the bio-fouled UXO. It is however very encouraging that the RVM output for the bio-fouled UXO (within the red contour) is well above that for all of the non-UXO.

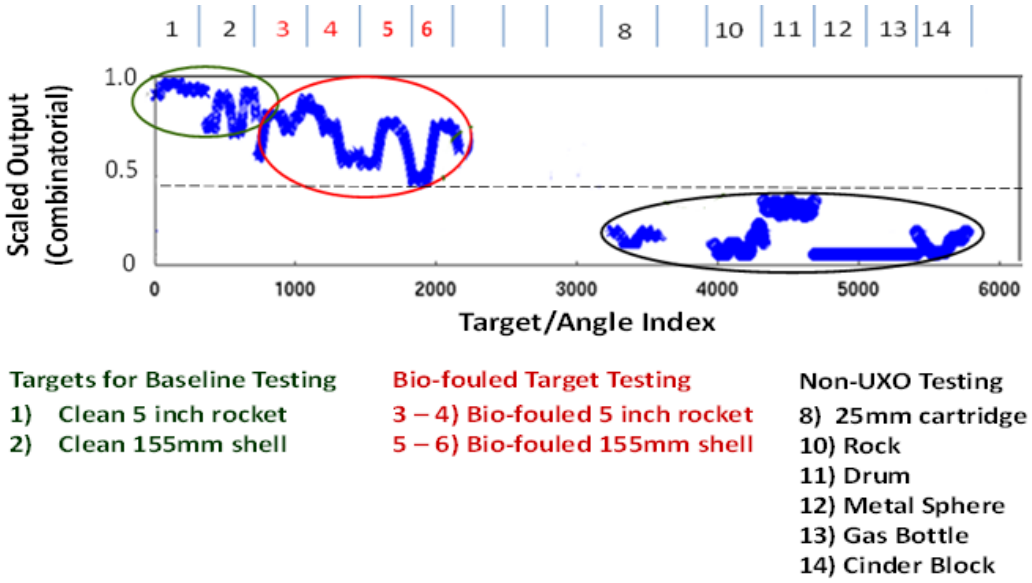

Figure 20. The performance (scaled combinatorial output) of the RVM classification algorithm trained generatively on even ½ degree angles using acoustic color for 5 inch and 155mm shells and tested on odd ½ degree angles for the 5 inch and 155mm shells and every degree for the bio-fouled target s and 6 non-UXO targets.

Next we present the low frequency acoustic scattering results for the lightly corroded shells. The acoustic color maps for the two corroded shells are shown in Fig. 21. As discussed previously, we observe very little change in the acoustic color maps due to this relatively thin corrosion level. The one exception to this is the structure seen at 0° and 180° (front and back) at very low frequencies i.e. about 4 kHz and below, and we comment on this after displaying the line plots below. In Figs. 22 – 25 are shown the 0°, 180°, 90°, and 45° line plots for the corroded five inch shell. As can be seen, for scattering from the front and back and to a somewhat lesser degree for 45° there are only subtle changes in the spectral response. In the 90° case, the levels are unaffected, but the Rayleigh wave ring resonance dip is gone indicating some damping or de-coherence of the Rayleigh circumferential wave which seems surprising for such a thin corrosion layer.

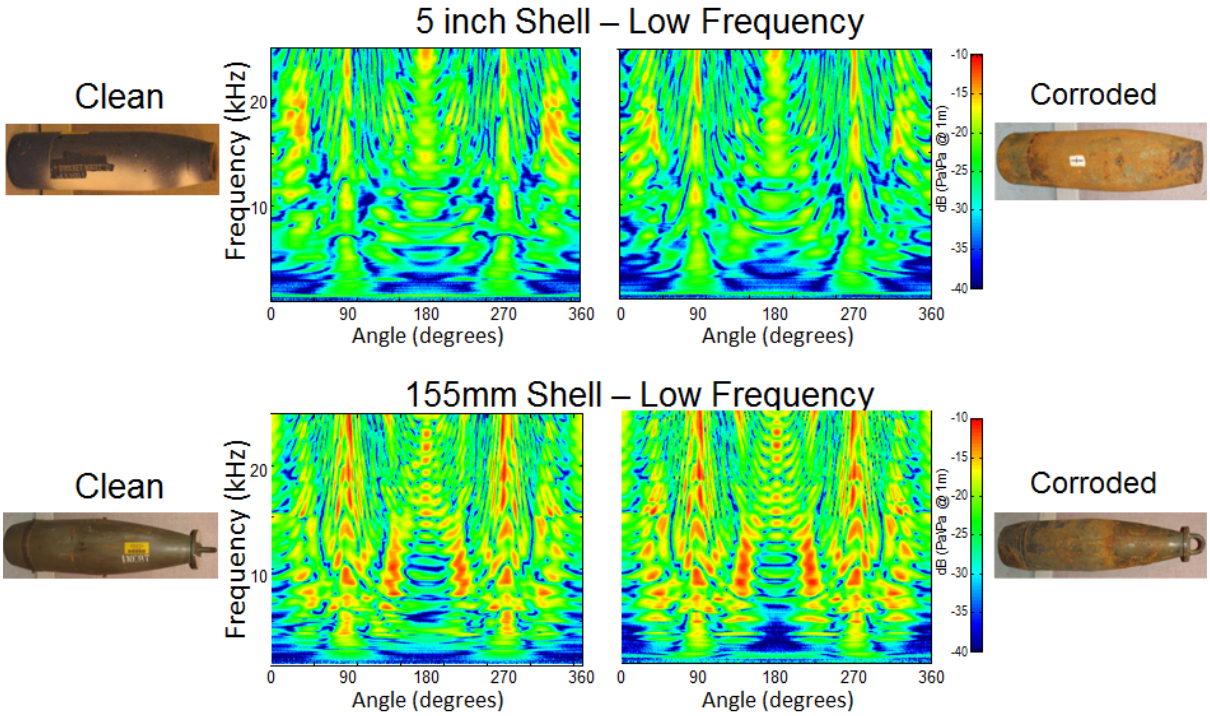

Figure 21. Measured acoustic color spectra for the clean and corroded shells: (upper) five inch shell; (lower) 155mm shell.

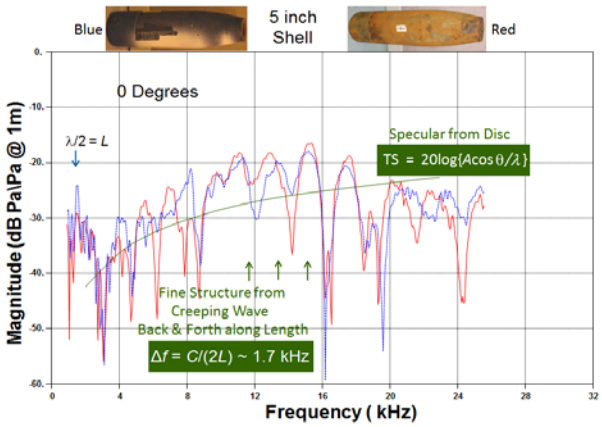

Figure 22. TS vs frequency for 5inch shell: (Blue) clean; (Red) corroded; (Green) theory for 1.4" radius rigid disc.

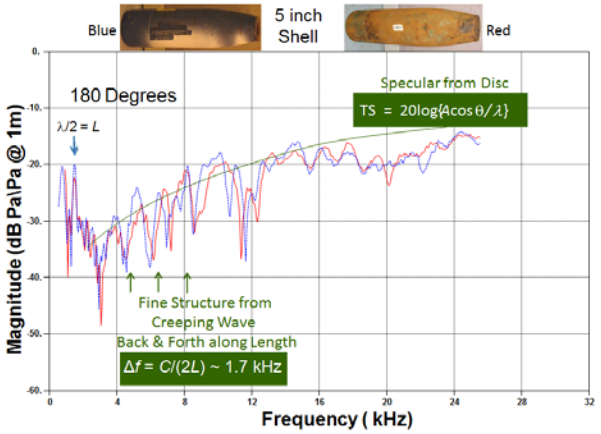

Figure 23. TS vs frequency for 5inch shell: (Blue) clean; (Red) corroded; (Green) theory for 2.5" radius rigid disc.

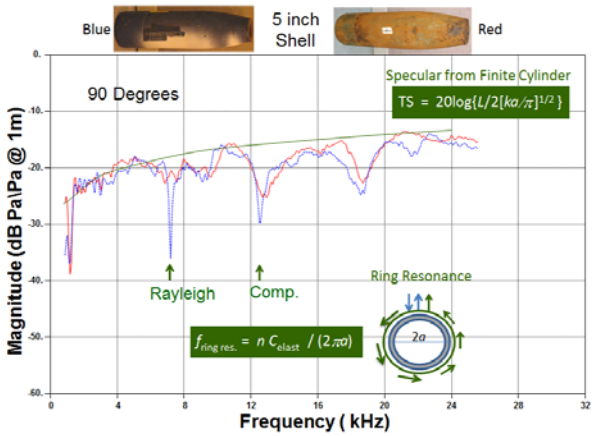

Figure 24. TS vs frequency for 5inch shell: (Blue) clean; (Red) corroded; (Green) theory finite rigid cylinder.

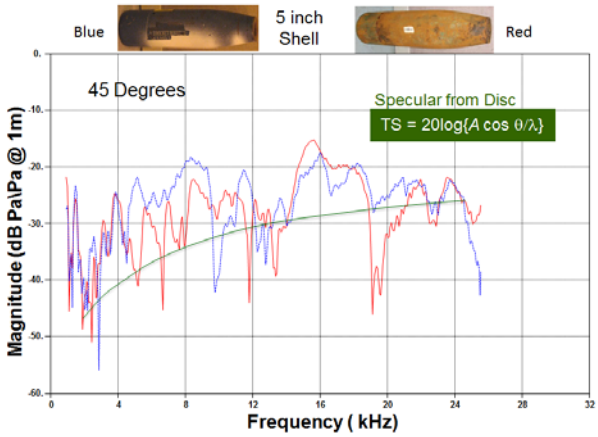

Figure 25. TS vs frequency for 5inch shell: (Blue) clean; (Red) corroded; (Green) theory for 2.5" radius rigid disc.

Next we show the corroded shell line plots for the 155mm shell in Figs. 26 – 29. The 0° case shown in Fig. 26 exhibits almost no change except for the aforementioned decrease at 4 kHz and below. This is even more the case for the 180° case shown in Fig. 27. The color maps shown in Fig. 21 illustrate that this drop-out has some extent in aspect angle. How such a thin corrosion layer can have such a large impact is unclear. In the 90° case, the clean and corroded cases are basically identical including the detail in the ring resonances. That the circumferential Rayleigh wave in the 155 shell appears unaffected by the thin corrosion layer is opposite to what was seen in the corroded 5 inch shell case, and we do not understand this contrast. Finally, the 45° response is also basically unchanged.

In summary, except for the apparently anomalous change for the echo from the front and back of both shells and the significant effect on the circumferential Rayleigh wave for the five inch shell, there is as expected no change of any consequence caused by this thin corrosion layer at the very low frequencies. We conclude without specifically demonstrating it that there would be little

impact on acoustic detection ranges, classification performance, or maximum burial depth caused by this thin corrosion layer.

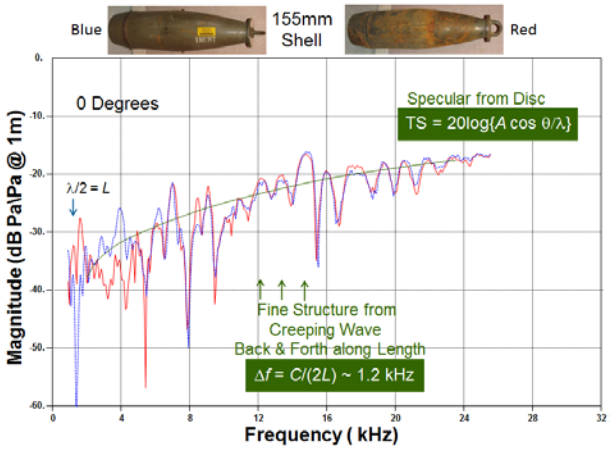

Figure 26. TS vs frequency for 155mm shell: (Blue) clean; (Red) corroded; (Green) theory for 2" radius rigid disc.

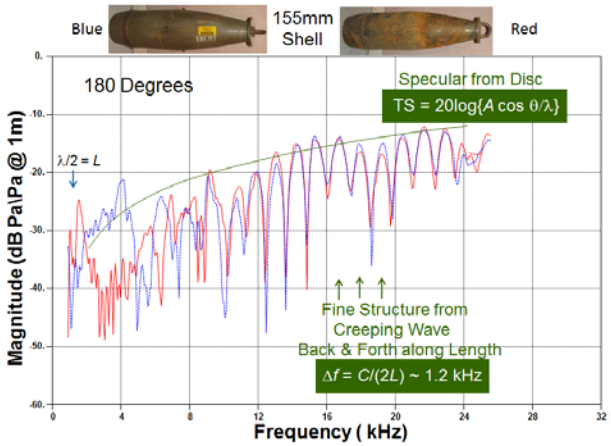

Figure 27. TS vs frequency for 155mm shell: (Blue) clean; (Red) corroded; (Green) theory for 2.62" radius rigid disc.

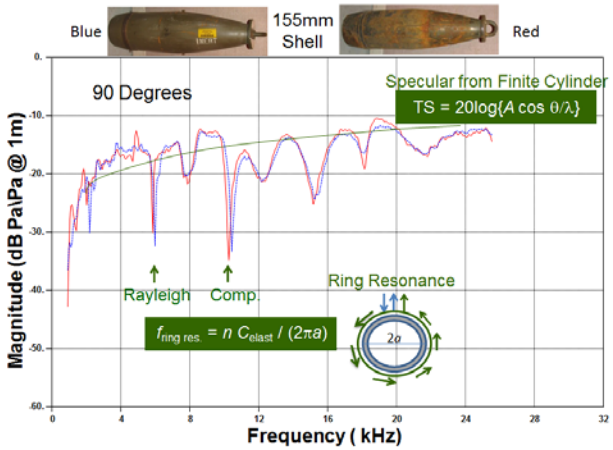

Figure 28. TS vs frequency for 155mm shell: (Blue) clean; (Red) corroded; (Green) theory for rigid finite cylinder.

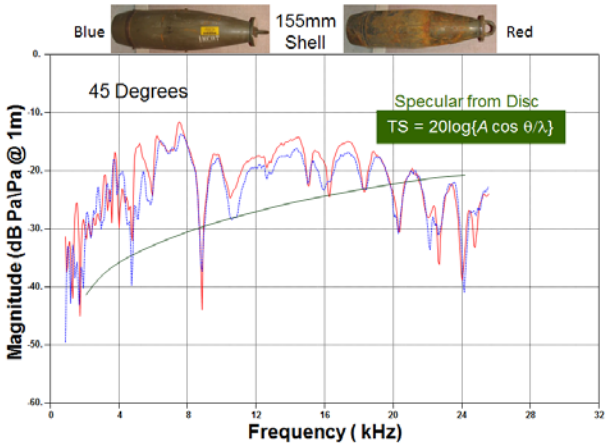

Figure 29. TS vs frequency for 155mm shell: (Blue) clean; (Red) corroded; (Green) theory for 2" radius rigid disc.

High Frequency Studies

Next we present the measurements made over the high frequency band 20 kHz - 160 kHz. Most of the focus to date in our previous SERDP research has centered on the "structural acoustics" regime (SA), the band from 2 kHz to 25 kHz as discussed in the previous section of this report. As can be clearly seen in Fig.1, the character of the acoustic color spectrum is rich in frequency-angle structure in this band which is directly related to a variety of scattering mechanisms. As further illustrated in the acoustic color display of Fig. 1, above the SA band, the echo response becomes much more related to what is called geometric scattering, i.e. one determined mainly by shapes and sizes and less by elastic phenomena. We present the following high frequency results both from an interest in being complete but also because this band is one in which high resolution sonars operate in search of proud and partially-buried targets. Regarding the latter, we are interested in determining whether bio-fouling or corrosion effects decrease UXO target strengths so as to diminish S/N and effective proud and partially buried UXO detection ranges

for these higher resolution sonars. We are also interested in surmising whether significant bio-fouling can blur the otherwise sharp images typically formed by these high resolution sonars.

We show the high frequency acoustic color maps for the clean and bio-fouled shells for both targets in Fig. 30. As can be seen, there are only subtle changes caused by the bio-fouling. To look at these in more detail, we present the line plots for the front, back, and side direction as a function of frequency.

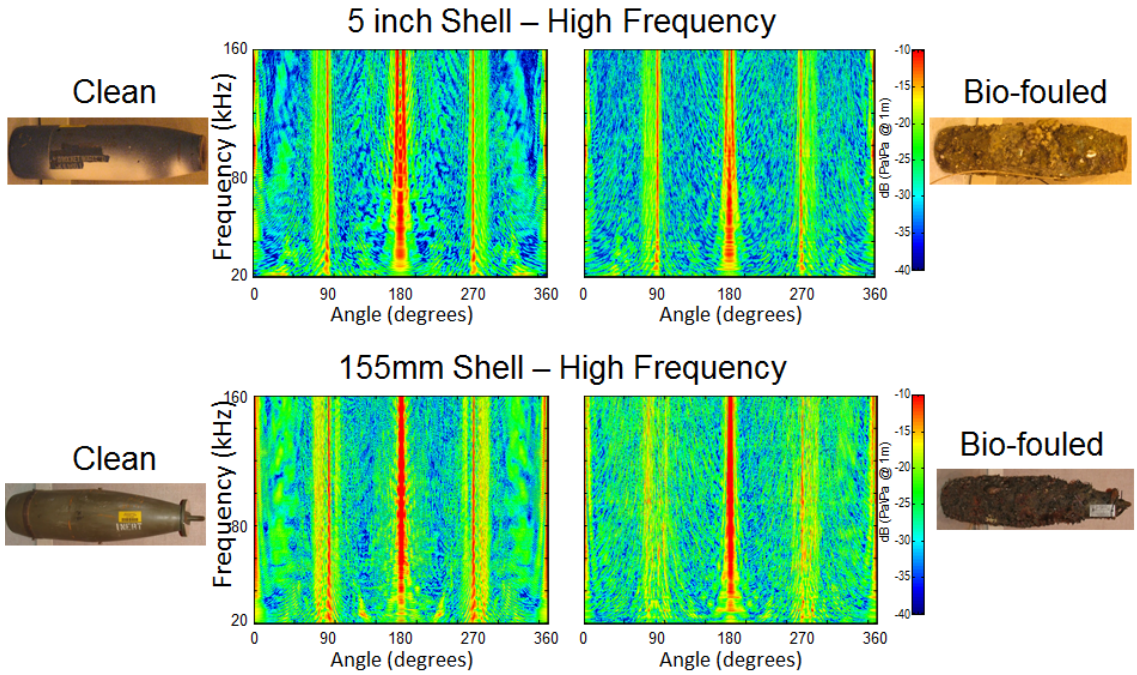

Figure 30. Measured acoustic color spectra for the clean and bio-fouled shells: (upper) five inch shell; (lower) 155mm shell.

We show the high frequency target strength for the clean and bio-fouled five inch rocket for 0° (target front) in Fig. 31 and for 180° (target back) in Fig. 32.

As can be seen for the 0° case, ignoring the broad 48 kHz modulation, the overall level and frequency shape is well explained by specular scattering from a rigid disc the size of the 5 inch rocket front as given by Eq. (1). As can be seen in the photo inset, the front end has a 1.57cm deep cavity at its center, and as predicted from Eq. (4) this cavity produces an interference structure whose periodicity is 48 kHz. This broad lobe structure is clearly seen in Fig. 31. Further, interference between the specular reflection and creeping waves travelling back and forth at the sound speed along the UXO length with 1.7 kHz fine structure as predicted by Eq. (4) is also clearly seen. Comparing the clean and bio-fouled results shows that there is very little change in the level or broad structure but that there is some reduction in the creeping wave component level.

Turning to the 180° case shown in Fig. 32, as outlined in the figure, the back end of this UXO has a concave structure which produces through interference a broad 125 kHz response lobe

which clearly drags down the overall disc-predicted response. Further, we see a large 7.6 kHz superimposed fine structure which is exactly predicted for a radial wave travelling down the length of the UXO with the compressional plate-wave speed and then reflecting back as it meets the discontinuity associated with the tapered radius. One can also see a hint of the axial creeping wave 1.7 kHz fine structure. Comparing the clean and bio-fouled results shows that there is very little change in the level or broad structure but that there is a significant reduction in the compressional wave 7.6 kHz fine structure level and a modest drop in the creeping wave fine structure.

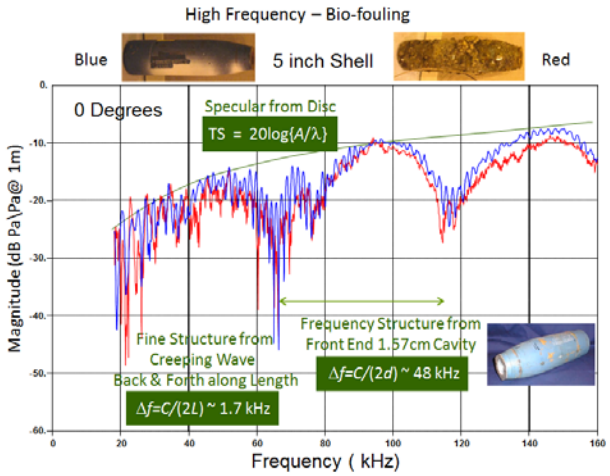

Figure 31. TS vs frequency for 5"shell: (Blue) clean; (Red) bio-fouled; (Green) theory for 1.4" radius rigid disc.

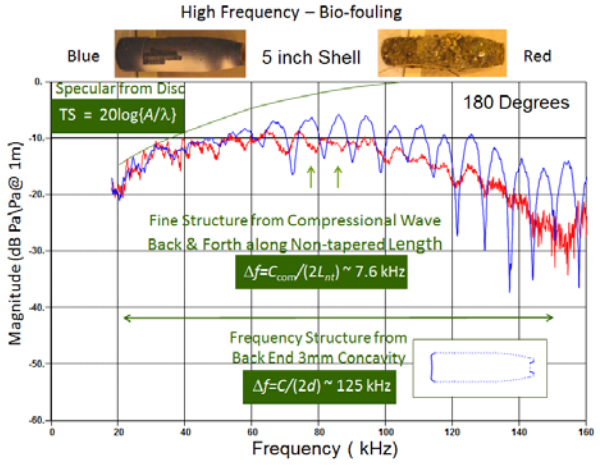

Figure 32. TS vs frequency for 5" shell: (Blue) clean; (Red) bio-fouled; (Green) theory for 2.5" radius rigid disc.

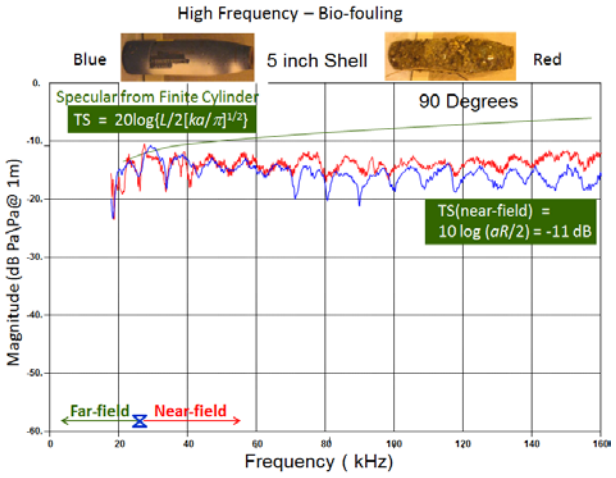

Figure 33. TS vs frequency for 5"shell: (Blue) clean; (Red) bio-fouled; (Green) theory for finite rigid cylinder.

Next, we consider the beam response (90°) as shown in Fig. 33. The otherwise successfully applied rigid scattering expression in Eq. (2) is now seen to agree with the data and its rise with frequency at the low end of the band, but the

data then levels off and no longer increases as does the rigid model. As indicated in the lower left hand corner, at the receiver-to-target distances used in the measurements (3.7m), we enter the near field above about 25 kHz where the TS expression now shifts to one independent of frequency[23] viz.

$$\mathrm{TS}(\text{near-field}) = 10\log\left(\frac{aR}{2}\right). \qquad (5)$$

For the radius of the shell and measurement range, Eq. (5) predicts -11dB which is in good agreement with the TS value to which the measurements level off. We are not certain regarding which circumferential waves are responsible for the several narrow frequency drop outs seen in the middle of the band. Regarding the effect of bio-fouling, we see that now for the first time there is a modest increase in scattering level over the upper frequency half of the band which is probably due to the reduction of this circumferential wave and its destructive interference with the specular return.

Next, we show the high frequency target strength for the clean and bio-fouled 155mm shell for 0° (target front) in Fig. 34 and for 180° (target back) in Fig. 35. In both cases, the predictions from Eq. (1) for rigid disc scattering describe the measurements well except that the predicted levels are several dB higher. Similar to the other UXO, interference with creeping waves travelling back and forth along the length of the shell at the sound speed produce a 1.2 kHz fine structure at 0° whereas analogous axially travelling compressional waves produce 7 kHz fine structure at 180° in addition to the creeping wave 1.2 kHz fine structure. Regarding the effect of bio-fouling, similar to what was found for the five inch rocket, we see almost no drop in the overall levels but a significant drop in the axially propagating compressional and creeping waves.

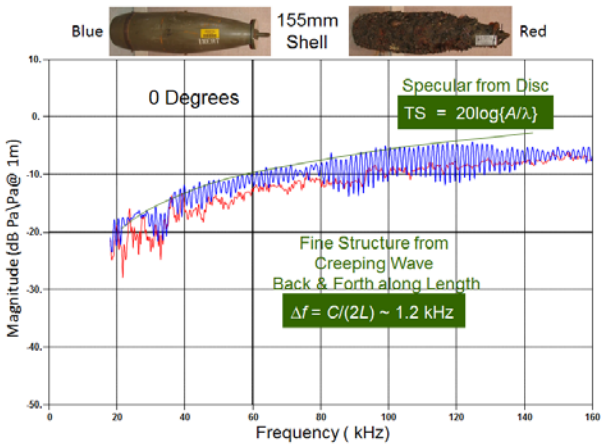

Figure 34. TS vs frequency for 155mm shell: (Blue) clean; (Red) bio-fouled; (Green) theory for 2" radius rigid disc.

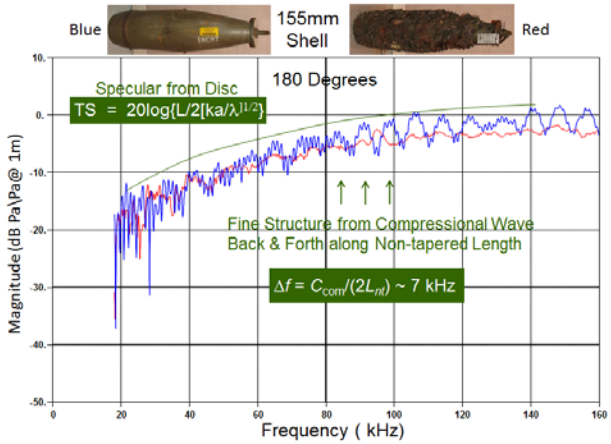

Figure 35. TS vs frequency for 155mm shell: (Blue) clean; (Red) bio-fouled; (Green) theory for 2.62" radius rigid disc.

Finally, we show the beam (90°) response for the 155mm shell in Fig. 36. As in the case for the other UXO, as we move beyond 20 kHz, the measurements are now in the nearfield and have become independent of frequency although slightly lower than predicted. In addition, there appears to be a small broad depression for the bio-fouled shell near 120 kHz from some unknown mechanism. We also see the drop-outs related to the at this point unknown ring resonances as in the previous case. Regarding the over-all effects of bio-fouling at high frequencies, the bio-fouling has resulted in a modest decrease in the overall level as well as a decrease in the influence of axial creeping and compressional waves.

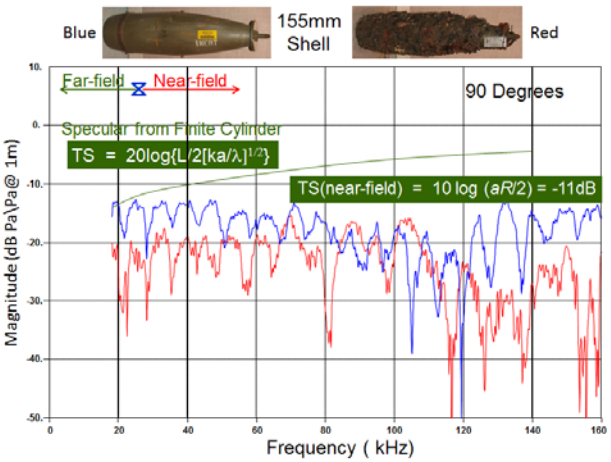

Figure 36. TS vs frequency for 155mm shell: (Blue) clean; (Red) bio-fouled; (Green) theory for finite rigid cylinder.

As we did with the low frequency data, we show in Fig. 37 angle-angle correlation maps based on the high frequency TS clean versus bio-fouled data. These plots are generated by computing the correlation co-efficient between the target strengths for two targets at each angle integrated over the entire low frequency band. We take as the baseline correlated cases the same clean targets (1 and 2) which show a a high correlation and as the baseline uncorrelated cases different targets either one of which is clean or bio-fouled (5 – 8). For the latter, we only show the correlation result for the two different clean targets (6). As can be seen, there remains a significant correlation diagonal for the two test cases, i.e. the clean versus the bio-fouled targets.

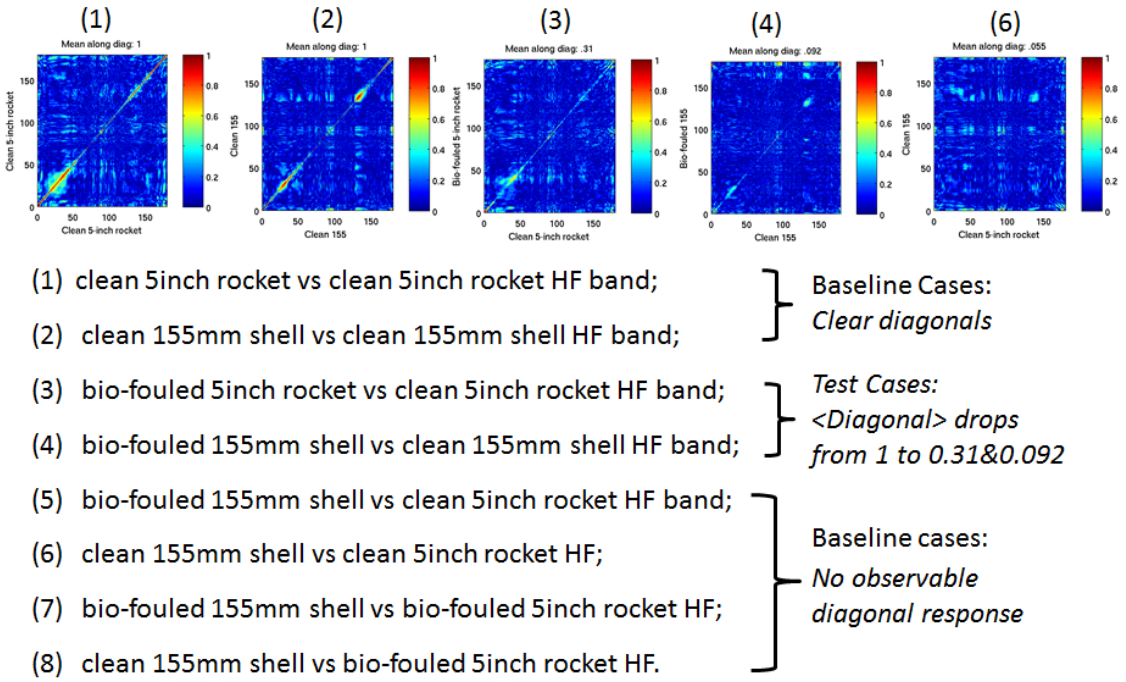

Figure 37. High frequency correlation co-efficient between TS of target 1 at θ_i and target 2 at

Next, we present the high frequency TS maps (acoustic color) for the corroded target responses for both the five inch and 155mm shells. As can be seen in Fig. 38, as expected there is very little difference between the color maps for the clean and corroded targets.

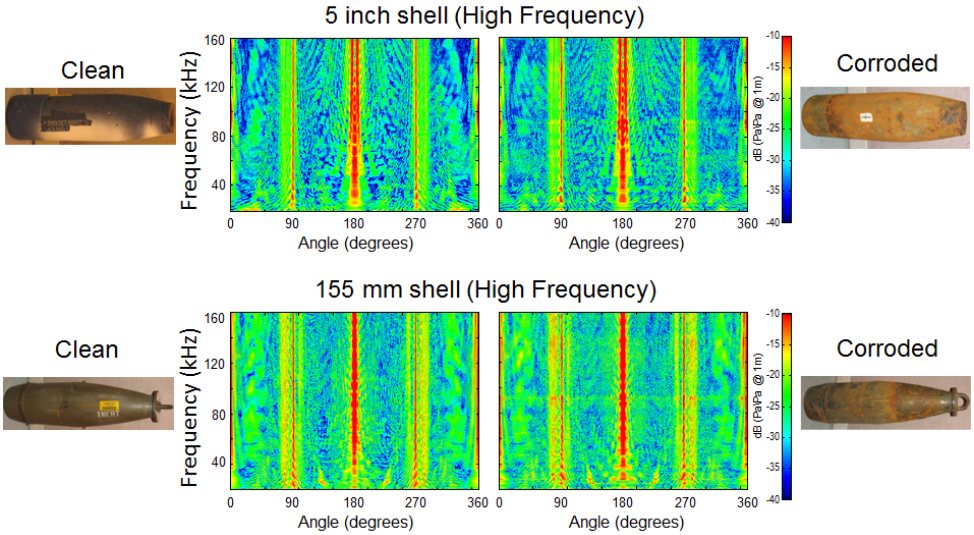

Figure 38. Measured acoustic color spectra for the clean and corroded shells: (upper) five inch shell; (lower) 155mm shell.

For completeness, we present the line plots for the usual angles for the clean and corroded targets in Figs. 39 – 44. All of these line plots confirm that there is really no experimentally significant differences detected over the high frequency band between the clean and corroded shells.

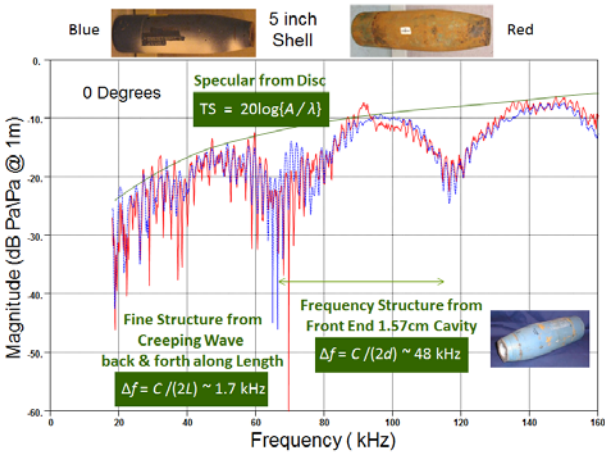

Figure 39. TS vs frequency for 155mm shell: (Blue) clean; (Red) bio-fouled; (Green) theory for 2.62" radius rigid disc.

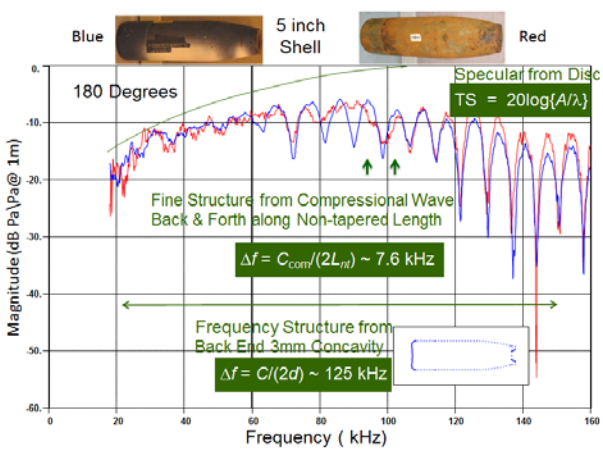

Figure 40. TS vs frequency for 5" shell: (Blue) clean; (Red) corroded; (Green) theory for 2.5" radius rigid disc.

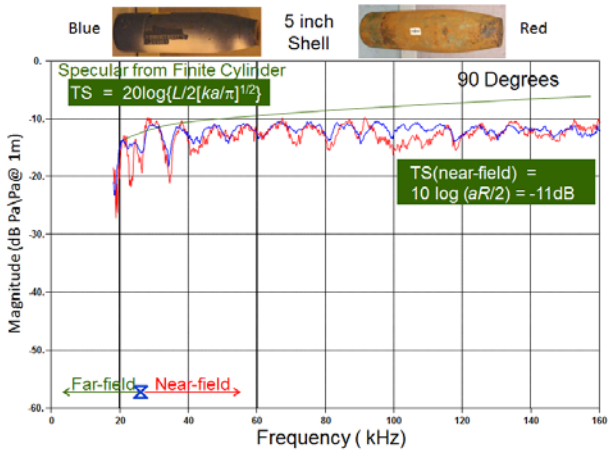

Figure 41. TS vs frequency for 5" shell: (Blue) clean; (Red) corroded; (Green) theory for rigid finite cylinder.

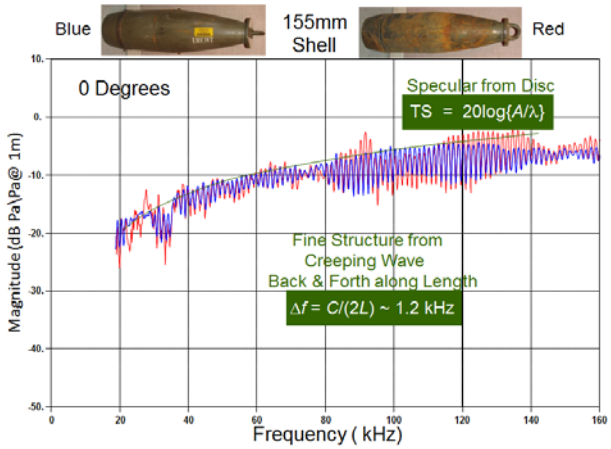

Figure 42. TS vs frequency for 155mm shell: (Blue) clean; (Red) corroded; (Green) theory for 2" radius rigid disc.

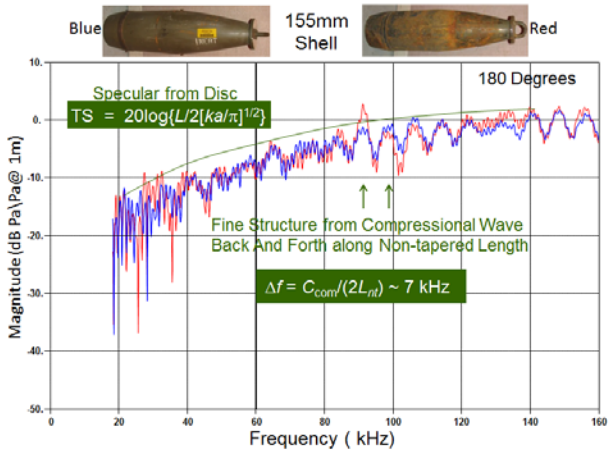

Figure 43. TS vs frequency for 155mm shell: (Blue) clean; (Red) corroded; (Green) theory or 2.62" radius rigid disc.

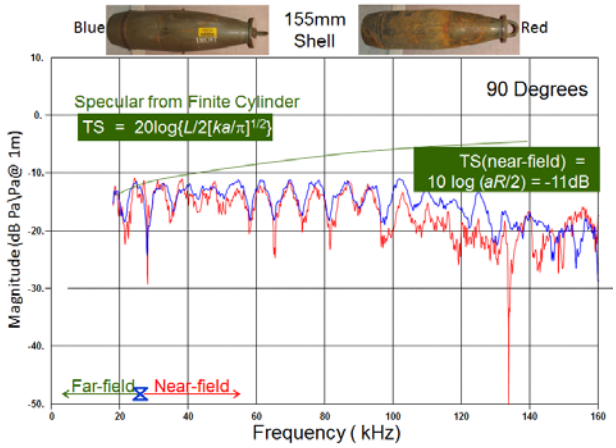

Figure 44. TS vs frequency for 155mm shell: (Blue) clean; (Red) corroded; (Green) theory for finite rigid cylinder.

CONCLUSIONS AND IMPLICATIONS FOR FUTURE RESEARCH/IMPLEMENTATION

In the case of bio-fouling, we were able to achieve substantial levels of fouling with a high percentage of hard fouling species so that significant bio-fouling occurred during this relatively short time (16 weeks). Contrasted with this, accelerated corrosion intended to produce magnetite/Hermatite corrosion layers by anodically polarizing the UXO in a bath of 0.05M NaCl for a week long period simulating ~3 months of seawater exposure achieved only a very this corrosion layer.

We can draw several conclusions from this limited but to our knowledge first study on the effects of bio-fouling and corrosion on the structural acoustic and acoustic response of two typical UXO. (1) Significant bio-fouling does not a have large impact on broadband echo characteristics

(acoustic color or target strength) and is not expected to degrade performance of existing RVM classification algorithms. (2) Significant bio-fouling is not expected to impact image quality. In some cases, it is expected to improve image quality by decreasing creeping and elastic wave contributions which corrupt the time delay beamforming processing used to form images. (3) Significant bio-fouling may (e.g. 155mm shell) or may not (e.g. 5 inch shell) decrease the detection range. In the former case, the several dB drop in the overall echo level would produce only a modest decrease in the depth at which buried targets could be prosecuted. (4) Light corrosion has no important effect on the acoustic echo data. Further corrosion studies should be carried out perhaps simulating long term corrosion by mechanically removing chunks of metal uniformly over the UXO surface.

LITERATURE CITED

1. J. A. Bucaro, B.H. Houston, M. Saniga, H. Nelson, T. Yoder and L. Kraus, and L. Carin, "Wide Area Detection and Identification of Underwater UXO Using Structural Acoustic Sensors," 1st Annual SERDP Report, NRL/MR/7130—07-9014, January 12, 2007.

2. J.A. Bucaro, B.H. Houston, M. Saniga, A. Sarkissian, H. Nelson, T. Yoder, L. Kraus, and L. Carin, "Wide Area Detection and Identification of Underwater UXO Using Structural Acoustic Sensors – 2nd Annual SERDP Report," NRL/MR/7130—08-9103, August 12, 2008.

3. J. A. Bucaro, B.H. Houston, H. Simpson, L. Kraus, T. Yoder, M. Saniga, A. Sarkissian, and L. Carin, "Wide Area Detection and Identification of Underwater UXO Using Structural Acoustic Sensors," 3rd Annual SERDP Report, January 2009.

4. J. A. Bucaro, B.H. Houston, H. Simpson , M. Saniga, A. Sarkissian, D. Calvo, L. Kraus, T. Yoder and L. Carin, "Wide Area Detection and Identification of Underwater UXO Using Structural Acoustic Sensors," 4th Annual SERDP Report, July 21, 2010.

5. J. A. Bucaro, B.H. Houston, H. Simpson, Z. Waters, M. Saniga, S. Dey, A. Sarkissian, D. Calvo, L. Kraus, and T. Yoder, "Wide Area Detection and Identification of Underwater UXO Using Structural Acoustic Sensors," Final Report SERDP Report, July 8, 2011.

6. Steven G. Kargyl and Kevin L. Williams, "Full Scale Measurement and Modeling of the Acoustic Response of Proud and Buried Munitions at Frequencies from 1-30 kHz," SERDP Project 1665 Final Report, May 2012.

7. J.A. Bucaro, A. Sarkissian, B.H. Houston, H. Simpson, Z.J. Waters, D. Anon, K. Jig, S. Liskey, and T. Yoder, "SERDP MR-2103 Interim Report, Dec. 2012.

8. J.A. Bucaro, A. Sarkissian, B.H. Houston, H. Simpson, Z.J. Waters, D. Amon, K. Jig, S. Liskey, and T. Yoder, "Structural Acoustic UXO Detection and Identification in Marine Environments – Final Report to SERDP MR-2103", April 10, 2014.

9. J.A. Bucaro, A. Sarkissian, B.H. Houston, M. Saniga, H. Simpson, Z.J. Waters, D. Amon, E. Williams, N. Valdivia, T. Yoder, K. Jig, and S. Liskey, "Structural Acoustic UXO Detection and Identification in Marine Environments – Interim Report for SERDP MR-2103 Follow-On", July 30, 2015.

10. J.A. Bucaro, A. Sarkissian, B.H. Houston, M. Saniga, H. Simpson, Z.J. Waters, D. Amon, E. Williams, and T. Yoder, "Structural Acoustic UXO Detection and Identification in Marine Environments – Final Report for SERDP MR-2103 Follow-On", May 31,, 2016.

11. Raymond Lim, "Data and Processing Tools for Sonar Classification of Underwater UXO," SERDP Project MR-2230 Final Report, August 2015.

12. B. H. Houston, J.A. Bucaro, T. Yoder, L. Kraus, and J. Tressler, J. Fernandez, T. Montgomery, T. Howarth, "Broadband Low Frequency Sonar for Non–Imaging Based Identification," IEEE Oceans 2002.

13. J.A. Bucaro, B.H. Houston, M. Saniga, L.R. Dragonette, T. Yoder, S. Dey, L. Kraus, and L. Carin, "Broadband Acoustic Scattering Measurements of Underwater Unexploded Ordnance (UXO)," J. Acous. Soc. Am. 123, 738-746 (2008).

14. Z. J. Waters, H.J. Simpson, A. Sarkissian, S. Dey, B.H. Houston, J.A. Bucaro, and T. Yoder, "Bistatic, Above-critical Angle Scattering Measurements of Fully Buried Unexploded Ordnance (UXO) and Clutter," J. Acous. Soc. Am., vol. 132, pp. 3076–3085 (2012).

15. Joseph A. Bucaro, Zachary J. Waters, Brian H. Houston, Harry J. Simpson, Angie Sarkissian, Saikat Dey, and Timothy J. Yoder, "Acoustic Identification of Buried Underwater Unexploded Ordnance Using a Numerically Trained Classifier," J. Acoust. Soc. Am. 132, 3614-3617 (2012).

16. Steven G. Schock, Arnaud Teller, Jim Wulf, Jason Sara, and Mark Ericksen, "Buried Object Scanning Sonar," IEEE J. Oceanic Eng. 26, 677-689 (2001).

17. S. G. Schock and J. Wulf, "Buried Object Scanning Sonar for AUV's," Oceans 2003, 494-499.

18. 8. Paul J. Carroll, "Underwater (UW) Unexploded Ordnance (UXO) Multi-Sensor Data Base (MSDB) Collection," Final report SERDP Project MM-1507, July 2009.

19. Robert A. Leasko, Charles L. Bernstein, Richard Holtzapple, and Jesse I. Angle, "Munitions Detection using Unmanned Underwater Vehicles Equipped with Advanced Sensors," Interim Report, ESTCP Project MR-201103, June 29, 2012.

20. M. Tipping, "Sparse Bayesian Learning and the Relevance Vector Machine," Journal of Machine Learning Research/, vol. 1, pp. 211-244, 2001.

21. J. A. Bucaro, H. Simpson, L. Kraus, L. R. Dragonette, T. Yoder and B. H. Houston, "Bistatic scattering from submerged unexploded ordnance lying on a sediment," The Journal of the Acoustical Society of America 126 (5), 2315-2323 (2009).

22. Daniel Steinhurst, Glenn Harbaugh, Matthew Strom, Joseph Bucaro, Thomas Bell, and Bruce Barrow, "Effects of Target Corrosion on Advanced EMI Signatures in Underwater Environments," SERDP Project MR-2500 Interim Report, December 2016.

23. R. J. Urick, *Principles of Underwater Sound*, 3rd ed. (McGraw-Hill, New York, 1983), pp 303 – 305.

24. H. Uberall, L. R. Dragonette, and L. Flax, "Relation between creeping waves and normal modes of vibration of a curved body, Journ. Acoust. Soc. of Am., 61, 711 (1977).

25. Gerard Maze, "Rayleigh wave Acoustic scattering from submerged cylinders. MIIR Im/Re: Experimental and Theoretical study," J. Acoust. Soc. Am. 89, 2559-2566 (1991).

26. Thomas D. Rossing and Daniel A. Russell, "Laboratory observation of elastic waves in solids," Am. J. Phys. 58, 1153-1162 (1990).

27. I. Ulusoy and C. M. Bishop, "Generative versus discriminative methods for object recognition," in Computer Vision and Pattern Recognition, 297 IEEE Computer Society conference (2005), Vol. 2, pp. 258–265.

ROUTE SHEET

CODE	DATE	INITIALS	•PURPOSE	REMARKS
7130	8/8	BH		
7102	8/8	MB		
7100	8/15	JS		
7102	8/15	MB		
~~1226~~ 1231	8/16/17	SF		
5596.3	8/22/17	Jeg		
1008.2	8/22	SC		
1030	8/24	AeH		
7102	8/31	MB		
7130	8/31	BF		

INSTRUCTIONS

Prepare 2 copies of this route sheet and forward ALL copies together with necessary correspondence and other documents

• PURPOSES

1. FOR INFORMATION
2. FOR APPROVAL
3. PREPARE REPLY
4. PREPARE ENDORSEMENT
5. FOR NECESSARY ACTION
6. FOR SIGNATURE
7. RETAIN ENCLOSURES
8. RETAIN COPY

NDW-NRL 5216/1030 (Rev. 2-82)

FROM

Code 7130, Physical Acoustics

DATE OF MATERIAL	BRANCH IDENT. SYMBOL
08-Aug-2017	NRL/MR/7130--10-0149

ORIG. IDENT. SYMBOL (*Mail Room Fill in*)

DIVISIONS DO NOT FILL IN

DATE MAILED

FILE NO.

SUBJECT

AUTHOR/TITLE: J.A. Bucaro, et.al., Effects of Target Corrosion/Bio-fouling on EMI & Structural Acoustic Signatures in Underwater Environments - Acoustic Component Final Report to SERDP MR-2500

R/S NO. (*Mail Room Fill in*)

Title of Publication:

Effects of Target Corrosion/Bio-fouling on EMI & Structural Acoustic Signatures in Underwater Environments – Acoustic

Component Final Report to SERDP MR-2500

17-1231-3007

NRLINST 5600.2

PUBLICATION APPROVAL

(Read instructions on Back Before Filling in Form)

TRACKING BAR CODE

PUBLICATION REQUISITION NUMBER (To be assigned by TID)	DIVISION REQUISITION NUMBER	BRANCH SERIAL NUMBER	DATE
	NRL/OT/7130--17-0149	7130-0049:jab	08-Aug-2017

1. PUBLICATION TYPE

(Check one) — PUB NUMBER (Assigned by Tech Info)

- ___ NRL Report
- x NRL Memorandum Report
- ___ NRL Publication
- ___ Other (Specify)

2. SECURITY CLASSIFICATION AND DOWNGRADING INSTRUCTIONS

[x] Unclassified [___] Secret [___] Formerly Restricted Data [___] UMDIS
[___] Confidential [___] Restricted Data [___] CNWDI

CLASSIFIED BY

DOWNGRADING

This publication (does not) (does) contain militarily critical technology

DIVISION HEAD NAME (First, MI, Last) — SIGNATURE

D.G. TODOROFF, SUPT, ACOUSTICS DIVISION

3. ORIGINATING DIVISION

PUBLICATION TITLE

Effects of Target Composition-Backing on SAR & Structural Acoustic Signatures in Underwater Environments – Acoustic Component Final Report to SERDP MR-2300

AUTHOR(S) NAME (First, MI, Last)

J. A. Bucaro, A. Sarkissian, B.H. Houston, and M. Saniga

Certification that copyright material meets requirements of NRLINST 5870.6A

Initial/Date

POINT OF CONTACT	CODE	EXT
J.A. Bucaro	7130	767-2491

JOB ORDER NUMBER(S)	SPONSOR AND PROJECT NUMBER(S)	FUNDS EXPIRATION OR EXTENSION DATE
71-9024-27	ESTCP/Misc. DoD 6.3	30 Sep 2018

4. ROUTING AND APPROVAL

ROUTING	SIGNATURE	DATE RECEIVED	DATE RELEASED	COMMENTS
B.H. Houston Author/COTR XXXX	A. Houston	8/8/17	8/8/17	
J.A Bucaro Section Head XXXXXXX				This is a Final Security Review. Any changes made in the document after approved by Code 1231, nullify the Security Review.
B.H. Houston Branch Head	A. Houston	8/8/17	8/8/17	
D.G Todoroff Division Head		8/15/17	8/15/17	
ADOR/Director NCST		8/15/17	8/15/17	
DOR/CO*	*(Do not forward to DOR/CO unless more than one Directorate is involved and/or NRL is affected as a whole (NRLINST 5600.2 Par 10a)			
Security 1231		8/16/17		
Publication Data Entry 5596.3	Judi Griffin	8/22/17	8/22/17	
Legal Counsel 1008.2	SC	8/22/17	8/22/17	
Public Affairs 1030 Unclassified/Unlimited Pubs Only		8/24/17	8	
Technical Information Production				

5. APPROVAL TO PRINT

Editorial				
Production				
Author(s)/COTR				

HQ-NRL 5291/1 (Rev 1-98) (Front)

PREVIOUS ISSUES OF THIS FORM ARE OBSOLETE

sponsor approval attached

6. DISTRIBUTION STATEMENTS ***(Author to check appropriate statement and fill in reason as required)***

[✓] A - Approved for public release, distribution is unlimited.

[ ] B - Distribution authorized to U.S. Government agencies only *(check reason below)*:

[ ] Foreign Government Information [ ] Contractor Performance Evaluation [ ] Critical Technology
[ ] Proprietary Information [ ] Administrative/Operational Use [ ] Premature Dissemination
[ ] Test and Evaluation [ ] Software Documentation [ ] Cite* Specific Authority _____ *(Identification of valid documented authority)*

Date statement applied _____

Other requests for this document shall be referred to _____ *(Insert Controlling DOD Office*)*

[ ] C - Distribution authorized to U.S. Government agencies and their contractors *(check reason below)*:

[ ] Foreign Government Information [ ] Software Documentation
[ ] Administrative/Operational Use [ ] Critical Technology [ ] Cite* Specific Authority _____ *(Identification of valid documented authority)*

Date statement applied _____

Other requests for this document shall be referred to _____ *(Insert Controlling DOD Office*)*

[ ] D - Distribution authorized to DOD and DOD contractors only *(check reason below)*

[ ] Foreign Government Information [ ] Critical Technology
[ ] Software Documentation [ ] Cite* Specific Authority _____ *(Identification of valid documented authority)*
[ ] Administrative/Operational Use

Date statement applied _____

Other requests for this document shall be referred to _____ *(Insert Controlling DOD Office*)*

[ ] E - Distribution authorized to DOD components only *(check reason below)*:

[ ] Proprietary Information [ ] Premature Dissemination [ ] Critical Technology
[ ] Foreign Government Information [ ] Software Documentation [ ] Test and Evaluation
[ ] Administrative/Operational Use [ ] Contractor Performance Evaluation [ ] Cite* Specific Authority _____ *(Identification of valid documented authority)*

Date statement applied _____

Other requests for this document shall be referred to _____ *(Insert Controlling DOD Office*)*

[ ] F - Further dissemination only as directed by _____ *(Insert Controlling DOD Office*)*

Date statement applied _____ or higher DOD authority _____

[ ] X - Distribution authorized to U.S. government agencies and private individuals or enterprises eligible to obtain export-controlled technical data in accordance with regulations implementing 10 U.S.C. 140c.

Date statement applied _____

Other requests for this document shall be referred to _____ *(Insert Controlling DOD Office*)*

**For NRL publications, this is usually the Commanding Officer, Naval Research Laboratory, Washington, DC 20375-5320*

7. OTHER LIMITATION

[ ] Classification only | NOFORN [ ] DTIC exempt *(explain)* _____

_____ Classification Review (Initial/Date)

Substantive changes made in this document after approval by Classification Review and Public Release invalidate these reviews. Therefore, if any substantive changes are made by the author, Technical Information, or anyone else, the document must be returned for another Classification Review and Public Release.

8. INSTRUCTIONS

Author completes and submits this form with the manuscript via line channels to the division head for review and approval according to the routing in Section 4.

1. NRL Reports	Submit the diskette (if available), manuscript, typed double-spaced, complete with tables, illustrations, references, draft SF298, and proposed distribution list.
2. NRL Memorandum Reports	Submit a copy of the original, typed manuscript complete with tables, illustrations, references, draft SF298, and proposed distribution list.
3. NRL Publications or other brochures, pamphlets, proceedings, or any other printed publications	Handled on a per case basis by Site Technical Information Office.

REPORT DOCUMENTATION PAGE	Form Approved OMB No. 0704-0188

1. REPORT DATE *(DD-MM-YYYY)*	2. REPORT TYPE	3. DATES COVERED *(From - To)*
26 06 2017	NRL Memorandum Report	

4. TITLE AND SUBTITLE	5a. CONTRACT NUMBER
Effects of Target Corrosion/Bio-fouling on EMI & Structural Acoustic Signatures in Underwater Environments – Acoustic Component Final Report to SERDP MR-2500	5b. GRANT NUMBER 5c. PROGRAM ELEMENT NUMBER
6. AUTHOR(S) J.A Bucaro, A. Sarkissian, B.H. Houston, M. Saniga	5d. PROJECT NUMBER 5e. TASK NUMBER 5f. WORK UNIT NUMBER

7. PERFORMING ORGANIZATION NAME(S) AND ADDRESS(ES)	8. PERFORMING ORGANIZATION REPORT NUMBER
Naval Research Laboratory 4555 Overlook Avenue S.W. Washington, DC	
9. SPONSORING/MONITORING AGENCY NAME(S) AND ADDRESS(ES) Strategic Environmental Research and Development Program (SERDP) Office 4800 Mark Center Drive, Suite 17D08 Alexandria, VA 22350	10. SPONSOR/MONITOR'S ACRONYM(S) 11. SPONSOR/MONITOR'S REPORT NUMBER(S)

12. DISTRIBUTION/AVAILABILITY STATEMENT

Approval for public release; distibution is unlimited.

13. SUPPLEMENTARY NOTES

14. ABSTRACT

This reports on the results of an experimental study focused on generating a carefully controlled data base determining the effects of corrosion and bio-fouling on a UXO's underwater echo characteristics, i.e. on "acoustic color" from which classification features and images are generated. The detailed frequency/angle structure in the measured acoustic color map provides effective "fingerprinting" features for the classification algorithm. Here we measure these color maps for two UXO – a 5" rocket and a 155mm shell both filled with an epoxy resin – and then repeat the measurements after the targets have experienced bio-fouling and then corrosion. Further, we attempt to determine how the various structural acoustic mechanisms which lead to these features are affected by the bio-fouling or corrosion.

15. SUBJECT TERMS

Underwater Buried UXO, structural acoustic target identification, sonar UXO detection, bio-fouled UXO, corroded UXO

16. SECURITY CLASSIFICATION OF:			17. LIMITATION OF ABSTRACT	18. NUMBER OF PAGES	19a. NAME OF RESPONSIBLE PERSON
a. REPORT	b. ABSTRACT	c. THIS PAGE			J.A. Bucaro
U	U	U	U	33	19b. TELEPHONE NUMBER *(Include area code)* 202-767-2491